

Future ocean warming may cause large reductions in *Prochlorococcus* biomass and productivity

Received: 8 May 2025

Accepted: 1 August 2025

Published online: 08 September 2025

 Check for updatesFrançois Ribalet¹✉, Stephanie Dutkiewicz^{2,3}, Erwan Monier⁴ & E. Virginia Armbrust¹

The cyanobacterium *Prochlorococcus* is Earth's most abundant photosynthetic organism and crucial to oceanic ecosystems. However, its sensitivity to a changing climate remains unclear. Here we analysed decade-long field measurements using continuous-flow cytometry from our SeaFlow instrument, collecting per-cell chlorophyll fluorescence and size data for ~800 billion phytoplankton cells across the tropical and subtropical Pacific Ocean to quantify the temperature dependence of cell division. *Prochlorococcus* division rates appear primarily determined by temperature, increasing exponentially to 28 °C, then sharply declining. Regional surface water temperatures may exceed this range by the end of the century under both moderate and high warming scenarios. Under these future conditions, our global ocean ecosystem model suggests a possible 17–51% reduction in *Prochlorococcus* production in tropical oceans. Even with the inclusion of hypothetical warm-adapted strains, models show significant production declines in the warmest regions, suggesting that thermal adaptation may not prevent negative impacts. These results highlight the potential vulnerability of *Prochlorococcus*-dependent marine ecosystems to future warming.

Global warming is pushing sea surface temperatures and ocean stratifications to record levels¹, with predictions that by 2100, much of the tropical and subtropical surface oceans will regularly exceed 30 °C (ref. 2). Such changes in ocean conditions threaten marine ecosystems, potentially leading to the extinction of key species due to profound and complex impacts on the competition and distribution of organisms³. Microscopic, unicellular phytoplankton are fundamental to the function of marine ecosystems as their photosynthesis generates the organic carbon consumed by other organisms. However, as future oceans warm and become more stratified and circulation patterns change, the flow of deep-water nutrients essential for phytoplankton growth may decrease^{4,5}, potentially favouring smaller phytoplankton species that are more efficient at nutrient uptake^{6,7}. This shift towards communities dominated by small phytoplankton is expected to alter

carbon cycling within ecosystems as their rapid turnover and slow sinking rates may lead to increased nutrient cycling in surface waters⁶, less efficient transfer of carbon to higher trophic levels and reduced sinking of organic carbon to the deep ocean⁸. And yet, our understanding of how small phytoplankton will respond to future ocean temperatures remains largely based on laboratory studies using model organisms^{9,10}, which cannot recapitulate the complexity of interactions and genetic diversity found in natural populations. Here we document the in situ thermal sensitivity of natural populations of the keystone cyanobacterium *Prochlorococcus*, revealing a decrease in division rate at high temperatures. Our numerical simulations predict that rising temperatures will decrease *Prochlorococcus* biomass production in future oceans, potentially triggering cascading effects throughout open ocean food webs.

¹School of Oceanography, University of Washington, Seattle, WA, USA. ²Department of Earth, Atmospheric, and Planetary Sciences, Massachusetts Institute of Technology, Cambridge, MA, USA. ³Center for Sustainability Science and Strategy, Massachusetts Institute of Technology, Cambridge, MA, USA.

⁴Department of Land, Air and Water Resources, University of California, Davis, CA, USA. ✉e-mail: ribalet@uw.edu

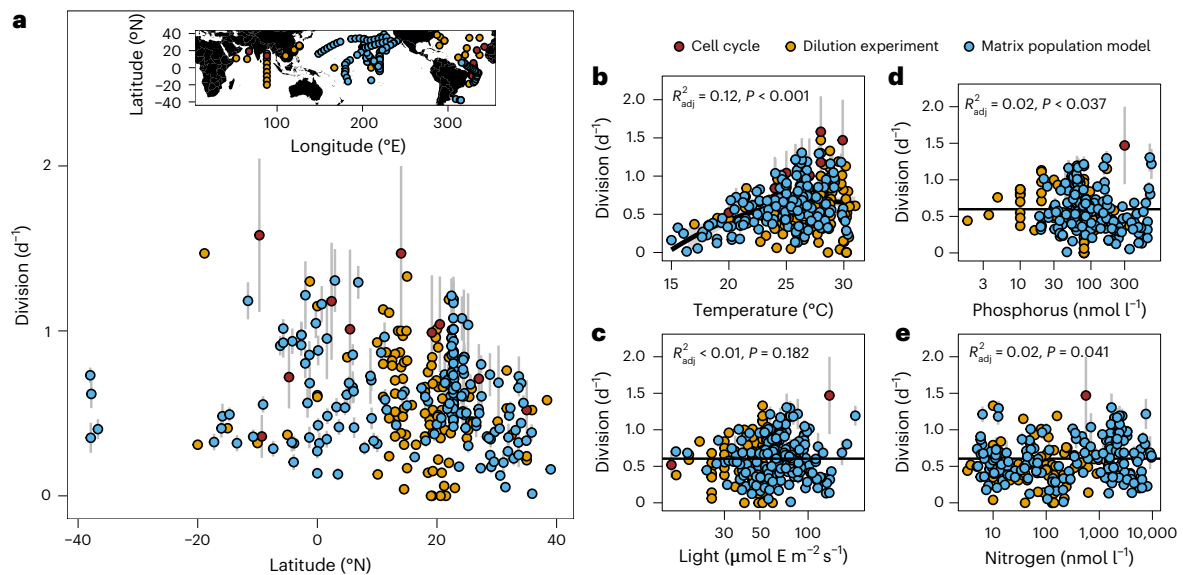


Fig. 1 | Global patterns in *Prochlorococcus* division rates (d^{-1}) in surface waters. **a**, Geographic distribution of daily division rates derived from the matrix population model ($n = 180$ independent samples), along with publicly available data from dilution experiments^{24,26–31} ($n = 103$ independent samples) and cell cycle analysis^{20,23–25} ($n = 11$ independent samples). The vertical bars represent methodological uncertainties associated with the matrix population model and cell cycle analysis; uncertainty estimates were not reported for dilution experiments. **b–e**, Relationships between division rates and environmental variables: daily average seawater temperature ($^{\circ}\text{C}$) (**b**), daily average photosynthetically active radiation (light, $\mu\text{mol E m}^{-2} \text{s}^{-1}$) (**c**) and phosphate (**d**) and nitrate (**e**)

concentrations (nmol l^{-1}). Temperature and light were directly measured in situ for all methodologies. Nutrient data sources varied by methodology: for the matrix population model, 21 out of 180 measurements came from direct observations and 159 out of 180 came from the Mercator-PISCES biogeochemical model; for cell cycle and dilution experiments, 65 out of 114 included measured nutrient data while the remainder was omitted from the plot. Statistical relationships were assessed using ordinary least squares regression with two-sided tests ($\alpha = 0.01$). The black line in **b** shows a second-order polynomial regression fit ($P = 5.746 \times 10^{-9}$), while the black lines in **c–e** show linear regression fits to the respective environmental factors. No adjustments for multiple comparisons were applied.

The cyanobacterium *Prochlorococcus* is the smallest (0.5–1 μm) and most abundant photosynthetic organism on Earth. It inhabits over 75% of the world's sunlit surface oceans, thriving in the nutrient-poor tropical and subtropical waters where it contributes nearly half of the phytoplankton biomass¹¹. Due to its small size and ability to genetically adapt to a wide range of environmental conditions¹², *Prochlorococcus* is predicted to reach even greater dominance in future warmer oceans owing to its potential range expansion towards the poles and an increased relative abundance under the low-nutrient conditions predicted for more stratified oceans^{13,14}. The extent to which these predictions based on laboratory experiments reflect the true thermal sensitivity of *Prochlorococcus* in diverse, more complex communities remains uncertain, partly owing to the limited availability of cell division rate estimates for natural populations, a challenge compounded by the difficulties of conducting non-disruptive measurements at sea¹⁵.

Results

In situ thermal limits of *Prochlorococcus*

Over the past decade, we have deployed our continuous-flow cytometer, SeaFlow¹⁶, on 90 research cruises, to collect per-cell fluorescence and light scatter data—optical measurements that reveal cell type and cell size, respectively—for approximately 800 billion phytoplankton cells less than 5 μm in size, including *Prochlorococcus* (Methods), across 200,000 km^2 of surface ocean¹⁷. We generated 180 cell division rate estimates for *Prochlorococcus* populations using hourly binned size distributions in a size-structured matrix population model¹⁸, a mathematical approach that tracks how cell size distributions change over time as cells grow and divide (Fig. 1, Supplementary Table 1 and Methods). These estimates are derived from changes in the relative cell size distribution rather than cell abundance, which avoids the confounding effects of mortality agents such as grazing. The model uses Bayesian inference and retains only estimates with strong model

fit and convergence, excluding those with abrupt changes in size distributions that can arise when sampling across different water masses containing *Prochlorococcus* populations with distinct cell sizes. This non-disruptive approach requires no manipulations or incubations, providing in situ division rates comparable to estimates from dilution experiments and cell cycle analysis^{19–22}. To broaden the spatial coverage of *Prochlorococcus*'s distribution range, we complemented our data with publicly available data from cell cycle analysis^{20,23–25} and dilution experiments that estimate *Prochlorococcus* division rates from shipboard incubations^{24,26–36} ($n = 114$; Extended Data Fig. 1).

Our results reveal high variability in the division rates of *Prochlorococcus* across latitudes, highlighting the complex interactions of temperature, nutrient and light availability on its growth (Fig. 1a) and motivating evaluation of the individual effects of each of these parameters. We observed a notable nonlinear relationship between division rate and temperature (Fig. 1b and Supplementary Table 2), with an initial increase in division rate followed by a decline at high temperatures, a pattern consistent across multiple cruises, locations and methodologies. A second-order polynomial regression fit to the data reveals a significant positive linear term (1.58 ± 0.28 , $P < 0.001$), supporting the previously observed increase of division rate with temperature²⁰, but also a significant negative quadratic term (-0.85 ± 0.28 , $P = 0.003$). Light intensity and nutrient concentrations showed less pronounced effects within the observed ranges, with non-significant terms in their regressions (Fig. 1c–e and Supplementary Table 2). Across all environmental conditions, in situ division rates of *Prochlorococcus* never exceeded 1.6 d^{-1} , equivalent to a population doubling time of about 10.5 h, with the highest values observed in tropical Atlantic²⁴ and Indian Oceans²³.

Given the apparent impact of temperature on *Prochlorococcus* division rates, we analysed the maximum division rates (top 80%) across various sea surface temperatures for each method (that is,

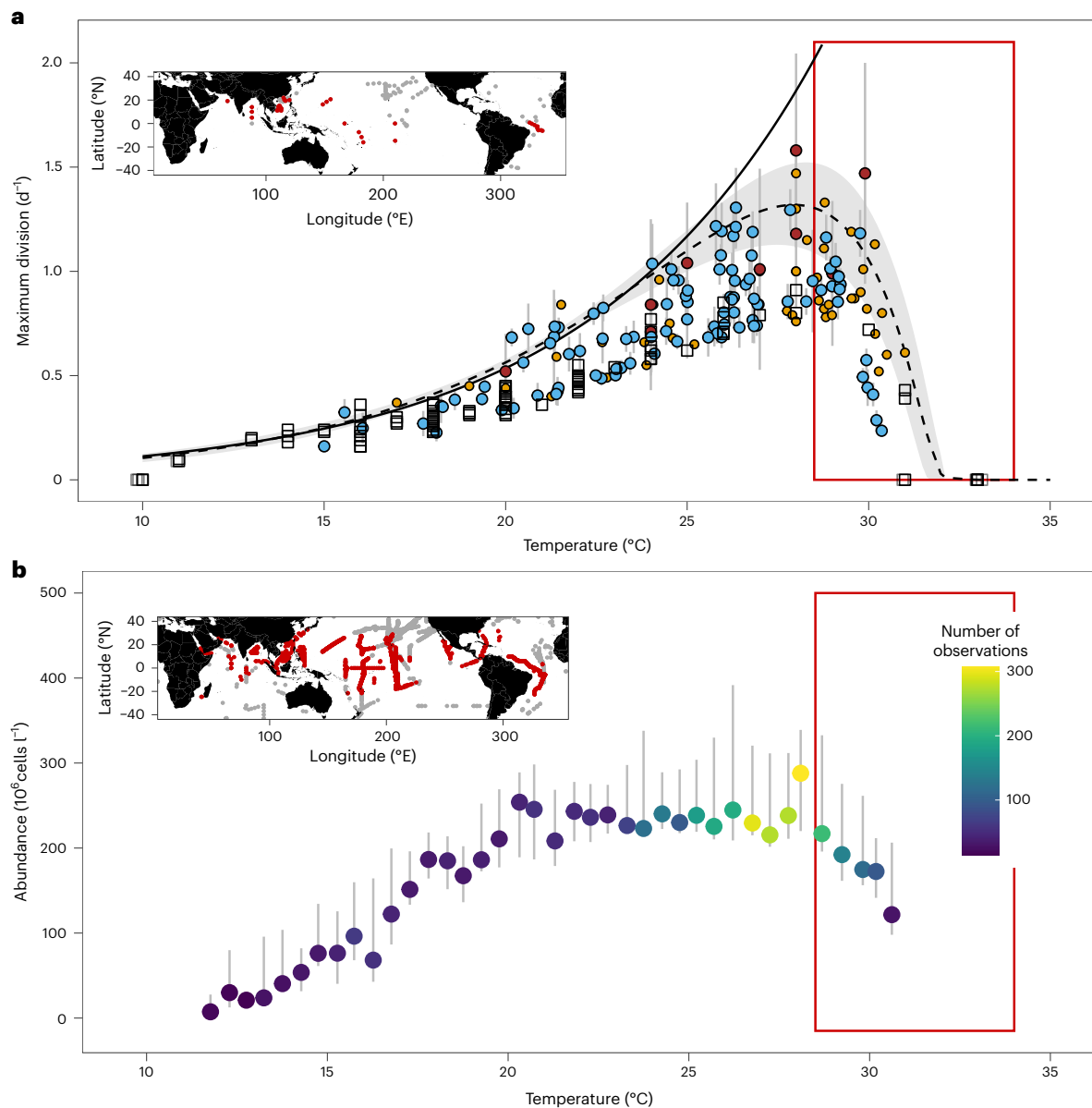


Fig. 2 | Temperature-dependent responses in *Prochlorococcus* populations.

a, Maximum division rate (top 80%, d^{-1}) of field populations, estimated from the matrix population model ($n = 100$ independent samples, blue circles) and from data compilations of dilution experiments^{24,26–36} ($n = 45$ independent samples, orange circles), cell cycle analysis^{20,23–25} ($n = 9$ independent samples, red circles) and culture isolates^{37–39} ($n = 94$ independent samples, white squares) grown under nutrient-replete conditions, plotted as a function of daily average seawater temperature ($^{\circ}C$). The solid and dashed lines represent the 99th quantile regression fits using a standard exponential curve and a metabolic theory approach, respectively. Shading around the dashed line indicates

the standard deviation of 1,000 bootstrap replicates. **b**, Cell abundance (10^6 cells l^{-1}) as a function of temperature, where points represent the median values of the top 80% of abundance measurements observed at each temperature bin. Data combine hourly binned SeaFlow measurements and compiled datasets^{14,23,43}, with colour coding representing the number of observations at each temperature. The error bars show the 5th and 95th percentiles within the top 80% subset. The red boxes highlight the observed detrimental effects of warm temperatures on the organism ($>28^{\circ}C$). The inset maps show the geographical distribution of sample locations, with samples collected in water above $28^{\circ}C$ indicated in red.

the matrix population model, dilution experiments and cell cycle analysis) (Fig. 2a). This approach minimized potential confounding effects of the methodology and environmental conditions to better determine the upper limit of the division rate at a given temperature (Extended Data Fig. 2). The analysis revealed that maximum division rates increased exponentially with rising temperature up to an in situ threshold of approximately $28^{\circ}C$. Above this temperature, maximum division rates declined sharply, with a nearly threefold reduction by $31^{\circ}C$, comparable to rates observed at $-19^{\circ}C$. This decline appeared primarily driven by temperature (generalized additive

model: $P < 0.001$; generalized linear model: $P < 0.004$), while the effects of photosynthetically active radiation (PAR) and phosphorus and nitrogen concentrations were not statistically significant within the observed ranges (Extended Data Fig. 2 and Supplementary Table 3). Importantly, we have not observed the high division rates predicted by exponential thermal curves ($>2.5 d^{-1}$ at $30^{\circ}C$; solid line in Fig. 2a) even in warmer regions such as the Indian Ocean, where nutrient conditions are more favourable (Extended Data Fig. 2), further supporting our findings of thermal limits in *Prochlorococcus* communities. Although environmental factors interact in complex

ways and are difficult to disentangle in natural phytoplankton communities, the field-observed patterns mirrored the thermal responses of 13 *Prochlorococcus* culture isolates grown with sufficient light and nutrient-replete conditions^{37–39} (Fig. 2a). We should note that only 2 of these 13 isolates originated from regions where annual mean sea surface temperatures exceed 28 °C, indicating that our culture collection does not fully represent *Prochlorococcus* from the warmest waters (Extended Data Fig. 3). Similarly, most of our field measurements come from cooler subtropical waters rather than warmer tropical regions, so we might be missing important data on *Prochlorococcus* that live in the hottest parts of the ocean. Despite this geographical sampling bias, culture isolates often show broader temperature tolerances than their isolation environment would suggest⁴⁰. The slightly lower division rates in cultures compared with natural populations further highlight the challenge of extrapolating laboratory findings to natural communities, as culture conditions cannot fully replicate the complex interactions with other marine microorganisms that influence *Prochlorococcus* growth in its natural environment. Notwithstanding these inherent limitations in both field sampling coverage of the warmest ocean regions and laboratory culture representation, the remarkable consistency between laboratory cultures and field observations across different methodologies and ocean regions indicates that *Prochlorococcus* growth rates probably do not increase exponentially beyond a temperature threshold of approximately 28 °C (solid line in Fig. 2a).

Prochlorococcus loss at high temperatures

The thermal sensitivity observed in natural populations of *Prochlorococcus* can be captured using a metabolic reaction function (dashed line in Fig. 2a), which incorporates the thermal sensitivity of enzyme kinetics, directly linking temperature changes to changes in metabolic rates¹⁰. This unimodal thermal response better captures *Prochlorococcus* temperature dependence than the traditional exponential curve approach (mean squared error of 0.11 and 0.79, respectively) that uses a Q_{10} temperature coefficient—a measure of how much growth rate changes with a 10 °C increase (solid line in Fig. 2a, Supplementary Fig. 1 and Supplementary Table 4). However, this Q_{10} function fits better for *Synechococcus*, the second smallest phytoplankton, across many ecotypes (Extended Data Fig. 4). The Q_{10} formulation also fits better for species groups within other taxa (for example, diatoms, coccolithophores)^{41,42}. By contrast, the exponential curve predicts unrealistically high maximum division rates for *Prochlorococcus* above 28 °C (solid line in Fig. 2a), overlooking its actual thermal sensitivity.

Building upon these observations, we investigated the relationship between slower division rates at higher temperatures and population abundances by combining our hourly average *Prochlorococcus* cell abundance data ($n = 12,814$) with those from compiled datasets^{14,23,43} ($n = 5,386$). We identified three distinct thermal responses: below 19 °C, *Prochlorococcus* abundance maxima (top 80%) increased exponentially with temperature; between 19 °C and 28 °C, abundance maxima leveled off despite exponentially increasing division rates, suggesting a proportional increase in mortality rates (Fig. 2a); and above 28 °C, maximum abundances began declining, with cell abundances reduced about twofold by 30 °C (Fig. 2b). *Synechococcus* abundances did not show a similar decline at high temperatures (Extended Data Fig. 5), maintaining populations in waters above 28 °C where *Prochlorococcus* abundances decrease. This differential response provides additional evidence against nutrient limitation as the primary driver of decline. If nutrient limitation at high temperatures were responsible, we would expect *Synechococcus*, with larger cell sizes and higher nutrient requirements, to be more severely affected than *Prochlorococcus*. This contrasting pattern supports our findings that direct temperature stress, rather than nutrient limitation, is the dominant factor causing the observed decline in both *Prochlorococcus* division rates and abundance at the warmest ocean regions.

Predicted *Prochlorococcus* future under climate change

We explored how our findings might affect future ocean ecosystems by integrating the observed *Prochlorococcus* thermal sensitivity into a comprehensive three-dimensional numerical ecosystem model within a global circulation framework⁴². The model simulates the distribution and fitness of many functional groups, including heterotrophic bacteria, autotrophs, mixotrophs and zooplankton types, linking physiological traits to biogeochemical function and cell size through size-dependent power laws (Supplementary Fig. 2 and Methods). Changes in population biomass are based on growth, grazing, mortality, sinking, and ocean fluid dynamics and mixing effects⁴⁴. For all functional groups except *Prochlorococcus*, we incorporated exponential thermal response curves (Supplementary Fig. 3 and Supplementary Table 4) for both growth and grazing rates. This Q_{10} parameterization aligns with previous studies for all other autotroph functional groups, including *Synechococcus*^{45,46} (Extended Data Fig. 4). However, for *Prochlorococcus* specifically, we implemented the metabolic thermal response curve from our data, with decreased division rates above 28 °C (dashed line in Fig. 2, Supplementary Fig. 3 and Supplementary Table 4). To project future impacts, we compared a baseline ocean derived from pre-industrial conditions (1860; Methods) with end-of-century conditions under two different climate scenarios (Supplementary Table 5). The first scenario projects stabilized greenhouse gas concentrations at ~650 ppm CO₂ equivalent by 2100 (similar to the Representative Concentration Pathways RCP 4.5), while the second assumes high emissions leading to CO₂ equivalent concentrations of ~1,370 ppm by the end of the century (similar to RCP 8.5). These scenarios result in a 1.9 °C and 3.8 °C increase in average sea surface temperatures and a nearly 6% and 9% reduction in nutrient supply in the sunlit surface waters, respectively (Extended Data Fig. 6 and Methods).

Our model incorporating *Prochlorococcus*'s upper thermal limit predicts a substantial decrease in both depth-integrated biomass (Extended Data Fig. 7) and production (Fig. 3a,b,g,i and Extended Data Fig. 8) in the tropical regions where future surface temperatures are projected to exceed 28 °C for much of the year (Extended Data Fig. 6). By 2090–2100, *Prochlorococcus* production in tropical regions will decline between 17% and 51% depending on whether moderate or high warming scenarios unfold (Supplementary Table 6). Regions such as the Western Pacific Warm Pool face particularly severe impacts, with our model predicting a near-complete collapse of *Prochlorococcus* populations (Fig. 3g,i). Thermal stress, not decreased nutrient supply, drives this decline (Extended Data Fig. 9 and Supplementary Table 6), supporting our observations (Fig. 2b). Despite habitat expansion into warmer, higher latitudes, global *Prochlorococcus* production will decline by 10–37% depending on the climate scenario (Supplementary Table 6). These substantial changes exceed the interannual variability in model projections by an order of magnitude (Methods and Supplementary Table 6) and will occur even under a moderate warming scenario, highlighting the potential threat to these foundational organisms. These projections contrast sharply with simulations relying on the more typically used exponential thermal response curve (solid line in Fig. 2a, Supplementary Fig. 3 and Supplementary Table 4), which instead forecasts moderate increases in annual *Prochlorococcus* production (18–30% under different scenarios) (Fig. 3a,b,h,j, Extended Data Fig. 8 and Supplementary Table 6).

As *Prochlorococcus* declines owing to the unimodal nature of its thermal norm, our model projects a compensatory increase from *Synechococcus*, seen in both increased biomass (Extended Data Fig. 7) and production (Fig. 3c,d,k,m). This compensation appears the strongest in tropical regions, where *Prochlorococcus* decline is most severe, resulting in an 11–34% increase in mean depth-integrated annual *Synechococcus* production across climate scenarios (Supplementary Table 6). Notably, this pattern of *Synechococcus* thriving in the very regions where *Prochlorococcus* populations collapse, such as in the Western Pacific Warm Pool, further supports that temperature stress, not

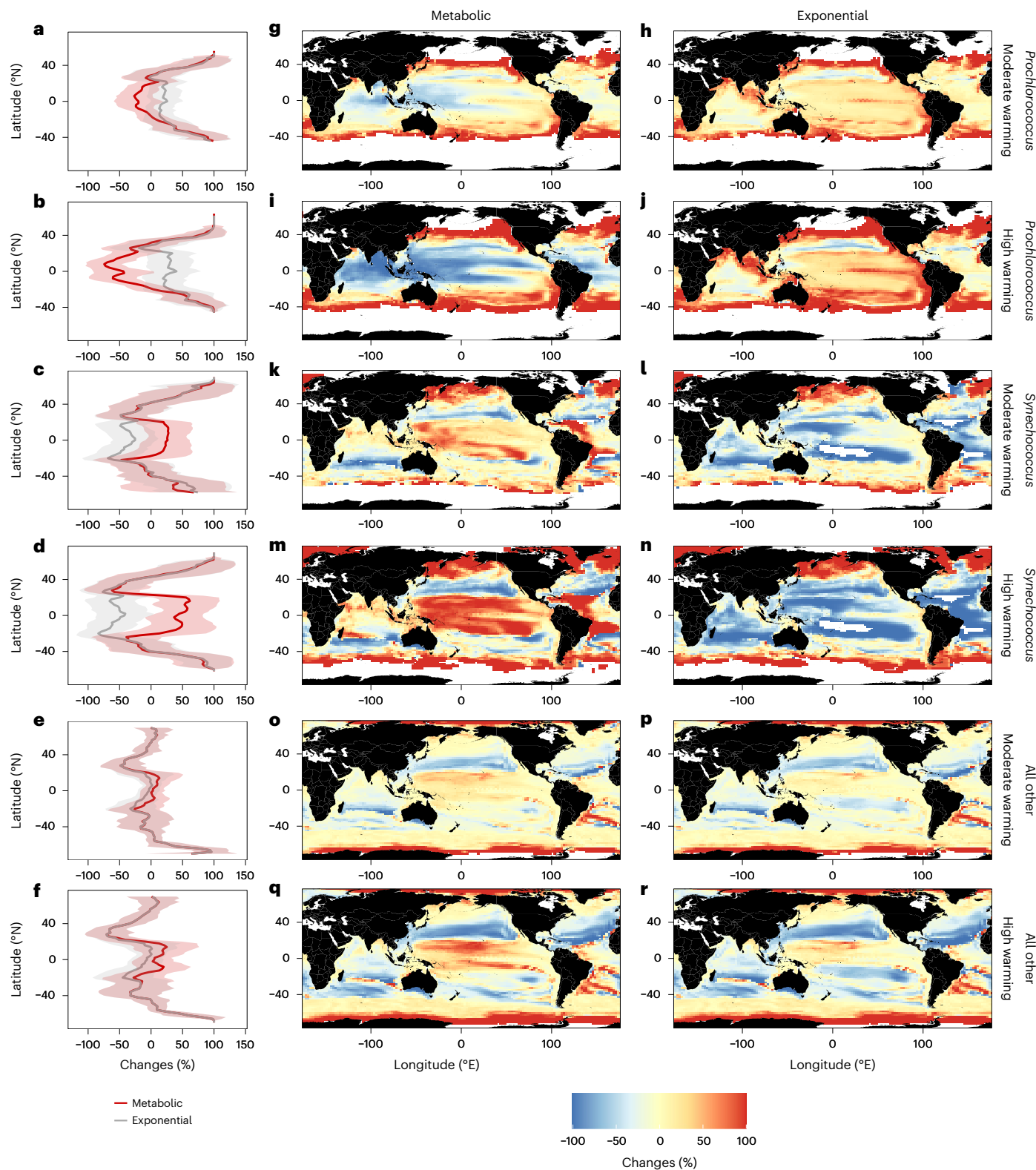


Fig. 3 | Projected changes in annual phytoplankton biomass production between pre-industrial (1860) and future (2090–2100) conditions, based on alterations in temperature, nutrient supply, mixing and ocean circulation anticipated under a moderate and high warming scenario. a–f, Latitudinal change (%) in depth-integrated biomass production for *Prochlorococcus* (a,b), *Synechococcus* (c,d) and all other phytoplankton (e,f) using either a standard exponential curve (grey) or a metabolic reaction approach (red) that relates the *Prochlorococcus* division rate to temperature, with shading representing

longitudinal variation from the mean (s.d.). **g–r,** The corresponding maps illustrate the percentage change in depth-integrated annual biomass production for *Prochlorococcus* (g–j), *Synechococcus* (k–n) and all other phytoplankton (o–r) projected under the two thermal norm assumptions and two climate scenarios. The white areas in **d–i** indicate that the phytoplankton type does not exist in those regions either pre-industrially or by the end of the century. Values of 100% increase indicate an expansion in the geographical range.

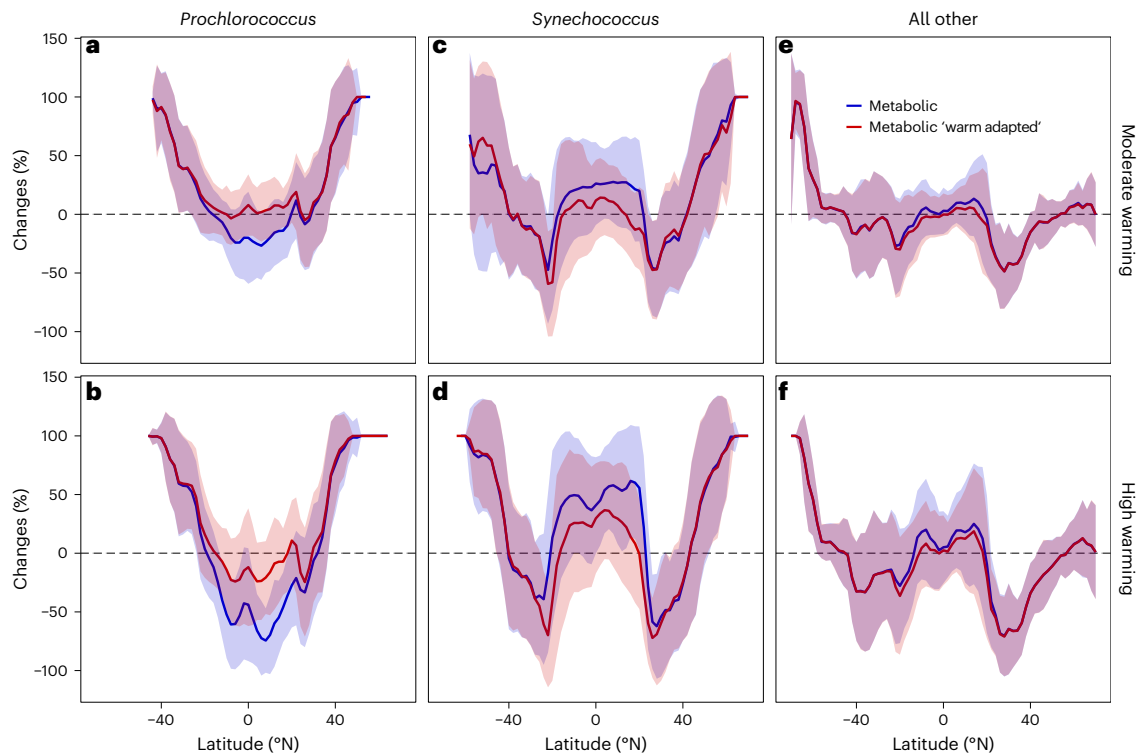


Fig. 4 | Impacts of a hypothetical warm-adapted *Prochlorococcus* strain on projected biomass production. a–f. Latitudinal change (%) in depth-integrated biomass production for *Prochlorococcus* (a,b), *Synechococcus* (c,d) and all other phytoplankton (e,f) comparing the standard metabolic reaction model (blue)

with a warm-adapted variant (red) for *Prochlorococcus*. The lines represent the mean across longitudes, and shading indicates longitudinal variation (\pm s.d.). Both projections use the same future climate scenario (2090–2100) and pre-industrial baseline (1860) as Fig. 3.

nutrient limitation, is the primary driver of *Prochlorococcus* decline. As warming enables range expansion towards the poles, global *Synechococcus* production increases by 5–20% depending on the climate scenario (Fig. 3c,d,k,m and Supplementary Table 6). Larger phytoplankton, primarily picoeukaryotes, show modest changes with production decreasing 4–7% (Fig. 3e,f,o,q and Supplementary Table 6). These results contrast sharply with projections assuming exponential *Prochlorococcus* temperature response, with a 15–26% decrease in *Synechococcus* production and a 6–11% decrease for larger phytoplankton across climate scenarios (Fig. 3c–f,l,n,p,r and Supplementary Table 6).

Thermal adaptation potential of *Prochlorococcus*

We created an *in silico* warm-adapted strain with an increased thermal tolerance to evaluate the potential impacts of *Prochlorococcus* populations adapted to warmer temperatures that were not included in the current metabolic response model. We reasoned that these warm-adapted populations could come to dominate future oceans either because they currently exist within regions not covered in our current dataset or because they emerge over time through adaptation or mutation and selection in response to continued warming ocean conditions. We retained the metabolic response function for these warm-adapted strains, increasing the optimal temperature from 28 °C to 30 °C and the maximum division rates from 1.3 d⁻¹ to 1.6 d⁻¹ (Supplementary Fig. 4), a temperature shift comparable to that observed for *Synechococcus* following long-term thermal tolerance experiments⁴⁷. Given that nutrient limitation has been shown to lower optimal temperature and reduce division rates in diverse species of phytoplankton, including cyanobacteria⁴⁸, this thermal shift represents a reasonable upper bound on thermal adaptation in *Prochlorococcus*. At the global scale, replacement of the observed thermal sensitivity (Fig. 2a) with the enhanced thermal adaptation into our

global ecosystem model partially mitigates the negative impacts on *Prochlorococcus* production (Fig. 3), resulting in a projected 6% increase under moderate warming and a 7% decrease under high warming in global *Prochlorococcus* production (Fig. 4a,b, Extended Data Fig. 10 and Supplementary Table 6). Under the high warming scenario, *Synechococcus* production increased by only 2% when competing with warm-adapted *Prochlorococcus* strains (Fig. 4c,d) and the larger phytoplankton groups showed moderate production decreases (7–9%) under the same conditions (Fig. 4e,f). Enhanced temperature adaptation proved effective in maintaining *Prochlorococcus* populations in tropical regions where temperatures remained below the warm-adapted strain's temperature threshold. However, even with increased thermal tolerance, significant production declines still occurred in the warmest tropical regions under the high warming scenario (15%; Extended Data Fig. 10 and Supplementary Table 6), suggesting that thermal adaptation may delay but not prevent the negative impacts of ocean warming on *Prochlorococcus*.

Discussion

The thermal sensitivity observed in natural populations of *Prochlorococcus* suggests fundamental physiological constraints that distinguish it from larger phytoplankton. Our findings show that *Prochlorococcus* division rates increase exponentially with temperature up to approximately 28 °C, then decline sharply at higher temperatures. This thermal response differs markedly from that of *Synechococcus* and other phytoplankton groups, whose growth rates continue to increase at temperatures where *Prochlorococcus* begins to decline.

This differential thermal sensitivity probably reflects distinct evolutionary histories and habitat adaptations. *Prochlorococcus* evolved in relatively stable tropical and subtropical environments where temperature fluctuations are minimal, potentially favouring resource efficiency over thermal versatility. Unlike coastal and

high-latitude phytoplankton that experience substantial temperature variations and maintain broader thermal tolerances, *Prochlorococcus* shows specific vulnerabilities at high temperatures. At 30 °C, *Prochlorococcus* isolates from warm regions such as the Sargasso Sea and Red Sea show suppressed photosystem gene expression⁴⁹ and disrupted circadian regulation⁵⁰, both critical for carbon fixation. By contrast, *Synechococcus* thrives at high temperatures, probably owing to proteomic adaptation that helps them minimize oxidative stress⁵¹ and resource reallocation strategies that maintain growth as temperature increases⁵². These physiological differences stem from divergent evolutionary trajectories: *Prochlorococcus* underwent genome streamlining, shedding many stress-response genes to minimize resource requirements while optimizing performance within a narrower environmental range. *Synechococcus*, however, maintains a more complex cellular machinery that, although costlier to maintain, provides greater resilience across variable conditions, including high temperatures. This evolutionary trade-off explains why *Prochlorococcus*, despite its dominance in stable nutrient-poor regions, may be more vulnerable to warming than *Synechococcus*.

These evolutionary trade-offs raise the critical question of whether *Prochlorococcus* can overcome its thermal limits in the near future. Despite its remarkable genetic diversity across ecotypes¹², the streamlined genome that enabled *Prochlorococcus* to dominate nutrient-poor waters may now limit its capacity to adapt to rapid warming, as evidenced by its reduced abundance in the warmest ocean region (Fig. 2b). Our model incorporating a hypothetical warm-adapted strain (with a 2 °C increase in thermal optimum) shows that adaptive evolution could partially buffer *Prochlorococcus* populations against warming impacts. However, even with this adaptation, significant declines are still projected in tropical regions, highlighting the limitations of evolutionary rescue when faced with rapid environmental change. For approximately 150 Myr, *Prochlorococcus* has evolved to thrive in nutrient-poor conditions, minimizing cell and genome sizes to reduce resource requirements, the very genomic streamlining that may now constrain its thermal adaptability. While *Prochlorococcus* probably persisted through past extreme climate events, such as the Early Eocene Climate Optimum when tropical seawater temperatures reached 35 °C (ref. 53), it probably did so by shifting polewards to cooler waters, a strategy that our ecosystem simulation also predicts for future warming (Fig. 3). Whether beneficial mutations could sweep through global populations within the timeframe of projected warming remains uncertain, especially given the unprecedented rate of anthropogenic warming and potential fitness trade-offs associated with thermal adaptation.

While our analysis provides evidence for thermal limits in *Prochlorococcus*, we must acknowledge several methodological limitations that complement the evolutionary considerations discussed above. Our field observations capture integrated responses of mixed communities rather than individual ecotypes, potentially masking the performance of rare, heat-tolerant variants. Strains with higher thermal tolerance may exist but remain uncommon owing to environmental trade-offs. Our sampling also presents geographic limitations. Laboratory studies disproportionately represent easily cultured ecotypes, with those from the warmest tropical regions remaining underrepresented (Extended Data Fig. 3). Similarly, while our field measurements spanned various ocean regions, many consistently high-temperature tropical areas remain unexplored. Despite these sampling limitations, our observations across the tropical Pacific consistently show reduced division rates at temperatures above 28 °C. The consistency of this pattern across diverse natural communities suggests a fundamental thermal limitation rather than an artefact of sampling bias. This thermal vulnerability demands serious consideration given *Prochlorococcus*'s global significance.

Prochlorococcus's thermal limitation potentially has profound implications beyond the species itself. The predicted decline of

Prochlorococcus could trigger cascading effects throughout marine food webs, particularly given the lack of functional redundancy within the *Prochlorococcus* ecological niche⁵⁴. While our model predicts some compensatory response from *Synechococcus*, the overall community shift would be substantial. As warming oceans favour larger phytoplankton expanding into the ecological niche currently occupied by *Prochlorococcus* (Fig. 3e,f,o,q and Extended Data Fig. 7), this fundamental shift at the base of the food web could alter the composition and abundance of grazers, impacting predators higher in the food chain⁵⁵, including fish populations⁵⁶. In addition, a reduction in *Prochlorococcus* populations may disrupt mutualistic relationships with other organisms such as SAR11 (ref. 57), the ocean's most abundant heterotrophic bacteria, potentially destabilizing the microbial community⁵⁸ and altering carbon cycling⁵⁹. Ultimately, a decline in *Prochlorococcus* production could have far-reaching consequences beyond a simple shift in species abundance, revealing the complex and interconnected nature of microbial communities. These findings underscore the importance of considering thermal constraints when projecting marine ecosystem responses to climate change, as our results suggest that *Prochlorococcus*, despite its ecological success and numerical dominance, may be sensitive to the temperature increases projected for tropical oceans in coming decades.

Methods

Phytoplankton abundance and composition

Data collection. We deployed the SeaFlow shipboard flow cytometer¹⁶ on 90 cruises from 2010 to 2023. The instrument continuously sampled seawater from the ship's underway intake, located at 3–8 m below the surface. Seawater was pumped through a 100- μ m stainless steel mesh filter to prevent clogging of the 200- μ m sampling nozzle. We continuously injected 1- μ m yellow-green Fluoresbrite microspheres (Polysciences) into the flow stream for scattering and fluorescence signal normalization. Particle emission was detected using two position-sensitive detectors for optimal focus determination. We measured red fluorescence (692/40 nm bandpass filter), orange fluorescence (572/28 nm bandpass filter) and forward light scatter (457/50 nm bandpass filter). Data were stored in 3-min intervals, yielding a sampling resolution of approximately 1 km along the cruise track (based on a ship cruising at ~20 km h⁻¹).

Data analysis. Raw data were processed to identify in-focus optimally positioned particles within the SeaFlow virtual core¹⁷. Optimally positioned particle analysis was performed using the R package Popcycle (version 4.7.3) available on GitHub. We defined five sets of gates based on forward light scatter, red fluorescence and orange fluorescence to identify 1- μ m beads, *Prochlorococcus*, *Synechococcus* and small eukaryotic phytoplankton (<5 μ m). Gate coordinates for each file were saved and stored in a structured query language (SQL) database. The equivalent spherical diameter (ESD) of each cell was estimated from forward scatter using the Mie light scatter theory. We then converted the ESD to carbon quotas using volume-to-carbon relationships for small phytoplankton¹⁷. *Prochlorococcus* size distributions were obtained by combining data collected every 3 min over each 1-h period ($n = 12,814$ hourly binned data points) to ensure robust statistical representation of the particle size distribution, with each hourly bin typically containing measurements from more than 10,000 individual cells.

Throughout our sampling campaigns, we validated SeaFlow cell abundance measurements against conventional flow cytometry (that is, BD Influx) for samples collected from both high- and low-temperature regions ($n = 683$; Supplementary Fig. 5). These validation efforts showed a good agreement between methods for *Prochlorococcus* abundance measurements across the temperature range, showing that dim *Prochlorococcus* cells in nutrient-poor warm waters were sufficiently resolved by our instrumentation for the purpose of this study.

Ancillary data. SeaFlow data were complemented with underway sea surface temperature measurements from shipboard thermosalinographs. These measurements were either broadcast in real time over the ship's network or retrieved from the Rolling Deck to Repository. The temperature data recorded simultaneously with SeaFlow measurements are available along with the SeaFlow data on GitHub (<https://github.com/seaflow-uw/seaflow-sfl/tree/master/curated>).

We complemented cell abundances derived from SeaFlow data with the Global Cyanobacteria dataset hosted on the Simons Collaborative Marine Atlas Project⁶⁰ (CMAP) database (that is, the tblFlombaum table), which contains global observations of *Prochlorococcus* abundance collected from 103 cruises¹⁴. As this dataset contains satellite-derived sea surface temperature data, we selected only samples from the upper 10 m to ensure appropriate temperature matching and excluded all zero values and empty entries ($n = 5,125$). We also incorporated two additional cruises in the Indian Ocean^{23,43} ($n = 261$) which included temperature data from the shipboard thermosalinograph. For these additional Indian Ocean datasets, we included all depth measurements with available temperature data.

Size-structured matrix model of division rates

Model parameters. We applied a size-structured matrix population model following the approach described in a previous study¹⁸, to estimate phytoplankton division rates. This category of model has shown its suitability for estimating in situ phytoplankton division rates for *Prochlorococcus*^{18,20}, *Synechococcus*^{19,61} and mixed populations of small eukaryotic cells^{22,62} in a wide range of environmental conditions, from estuarine to coastal to open ocean environments, and validated using culture experiments¹⁸, cell cycle analysis²⁰ and dilution experiments¹⁹. The latter indicates that the effects of size-specific mortality agents, if any, on the relative cell size distribution do not affect cell division estimation.

The size-structured matrix population model mechanistically simulates the evolution of the size distribution over a day–night cycle. The model discretizes cell counts across size classes and time using the parameter Δv and time using the parameter Δt . It quantifies the rates of the three key biological processes (cell division, carbon fixation and carbon loss), which are represented by the parameter vector $\theta = (\theta\delta, \theta\gamma, \theta\rho, \omega_0)$. These parameters, along with a concentration parameter σ (which allows for overdispersion in the data), determine the dynamics of the model. Below is a breakdown of the modelled processes:

- (1) Cell division (δ): Division rates are size dependent, reflecting the probability of cells transitioning to subsequent life-cycle stages. The model assumes a monotonically increasing division rate as a function of cell size.
- (2) Carbon fixation (γ): Carbon fixation rates are determined by light availability (PAR measurements) and cellular carbon content. This captures diel cycle dynamics and phytoplankton growth rates. The model incorporates a power–law relationship between carbon fixation and cell size.
- (3) Carbon loss (ρ): The model accounts for carbon loss through respiration and exudation, estimating rates separately for each size class. This reflects cell shrinkage due to metabolic processes other than division.

Prochlorococcus size distribution was obtained by combining data collected every 3 min over each 1-h period. These distributions were then discretized into 30 size classes based on the log of their carbon quotas, ranging from 80 fgC to 260 fgC per cell. This range was selected to fully encompass the variation in *Prochlorococcus* cell size observed in the SeaFlow dataset. We chose the volume bins and a time step of 10 min to ensure that cells would probably undergo only a single transition at a time within the model.

Data analysis. We used Bayesian inference, implemented through the Stan software package and Hamiltonian Monte Carlo algorithms, to process the data. A total of 6 Hamiltonian Monte Carlo chains were run for 2,000 Markov chain Monte Carlo iterations. This approach strikes a balance between computational efficiency and the complexity of our model. A list of model parameters and priors is available in Supplementary Table 1.

We implemented rigorous quality control measures to ensure accuracy and reliability of our model estimates. These measures included:

- (1) Model convergence: Samples with poor model convergence ($R\text{-hat} > 1.1$) were excluded, as this indicated potential unreliability of model-derived estimates⁶³.
- (2) Sample adequacy: Samples with insufficient cell counts (total number of particles counted over 1 h $< 10,000$) were excluded from analysis.
- (3) Data completeness: We excluded datasets with large gaps in temporal coverage (> 4 h).
- (4) Data integrity: We excluded 24-h periods containing abrupt shifts in cell size distributions. As phytoplankton cells typically increase their size by no more than a factor of two during a complete day–night growth cycle (that is, cells divide when they reach a critical size), larger or sudden changes in mean population size strongly indicate that we were sampling different populations with inherently distinct cell size characteristics. We detected these shifts using a change point detection method specifically developed for environmental flow cytometry data⁶⁴. While most of these shifts are usually filtered by our model convergence criteria, this additional step provided additional assurance that our estimates reflected genuine biological processes rather than sampling artefacts.
- (5) Biological consistency: We examined the correlation between carbon fixation patterns estimated by the model and division rates. As carbon fixation during daylight hours drives cell growth, which subsequently enables division, samples showing weak or absent correlations between these processes were flagged for potential anomalies, as this might indicate that factors other than normal physiological processes were affecting the size distributions.

Ancillary data. *Prochlorococcus* division rates were complemented with dissolved inorganic nutrient concentrations (nitrate plus nitrite and phosphate). For division rates obtained from the SeaFlow data, nutrient data were obtained mostly from Mercator-PISCES biogeochemical model forecasts ($\frac{1}{4}^\circ$ resolution), with 21 out of 180 data points from in situ measurements collected during research cruises in which the SeaFlow instrument was deployed. The PISCES model is a widely used tool for simulating marine biological productivity and the biogeochemical cycles of key nutrients (carbon, oxygen, phosphorus, nitrogen, silicon and iron) in the global ocean, and has been extensively validated against a wide range of available observations, including in nutrient-poor regions^{65,66}. Both in situ observations and model estimates are hosted in the CMAP database⁶⁰. The specific CMAP datasets for measured nutrient values were the following:

- tblKOK1606_Gradients1_Nutrients
- tblMGL1704_Gradients2_Nutrients
- tblKM1906_Gradients3_Organic_Inorganic_Nutrients
- tblTN397_Gradients4_NutrientsAndParticulates
- tblGradients5_TN412_NutrientsUW
- tblTN398_nutr
- tblHOT_CTD

and Mercator_Pisces_Biogeochemistry_Daily_Forecast_Nut for modelled data.

We extended our SeaFlow-derived *Prochlorococcus* division rates with a data compilation of in situ dilution experiments^{24,26–36} and cell cycle analysis^{20,23–25} (Extended Data Fig. 1). This dataset represents 114 estimates of *Prochlorococcus* division rates. For 65 out of 114 of these data points, measured environmental variables, including temperature, nitrate and phosphate concentrations, and PAR values, were provided directly within the compiled studies, based on field observations rather than model estimates or remote sensing data. These complementary datasets expand our geographic coverage beyond the North Pacific region where most SeaFlow deployments occurred, providing broader representation of different oceanic regimes.

We incorporated publicly available data on *Prochlorococcus* division rates derived from 13 different isolates cultured under nutrient-replete conditions^{37–39} (Extended Data Fig. 3). These isolates represent various ecotypes including both high-light- and low-light-adapted strains from different ocean regions. Of these 13 isolates, 2 originated from regions where annual mean sea surface temperatures exceed 28 °C, while others were isolated from cooler regions. This compiled dataset includes over 702 estimates of division rates under various temperature and light conditions. While isolate-based estimates are often lower than rates measured in situ, they provide valuable insights into physiological responses under controlled laboratory conditions and are used to test assumptions regarding how division rates respond to environmental variations.

Modelling the temperature response of the maximum division rate

Model parameters. The change in the cell division rate (μ) with temperature was characterized with either an exponential function (Eppley equation), an exponential function with mortality (Eppley–Norberg equation) or a metabolic theory of ecology (Hinshelwood equation), as described previously⁶⁷:

$$\mu = ae^{b(T-T_0)} \text{ (Eppley)}$$

$$\mu = ae^{b(T-T_0)} \left(1 - \left(\frac{T-T_c}{w/2}\right)^2\right) \text{ (Eppley–Norberg)}$$

$$\mu = A1e^{-E1/RT} - A2e^{-E2/RT} \text{ (Hinshelwood)}$$

where T represents the temperature and a represents the maximum division rates at T_0 (typically 20 °C), b is the exponential change in division rate with increasing temperature, T_c corresponds to the maximum of the quadratic portion of the equation, w is the thermal niche width (that is, the range of temperatures over which the division rate is positive), R is the gas constant (8.315 J mol⁻¹ K⁻¹), $A1$ and $A2$ are related to entropy and $E1$ and $E2$ are related to enthalpy.

Parameter estimation. To parametrize the coefficients, we fitted the 99th quantile regression to capture the division rate maxima at a given temperature. The 99th quantile is commonly used studying phytoplankton response to temperature, as it helps identify the upper limits of its thermal tolerance^{41,68}. Parameters were estimated using a least squared approach and a differential evolution algorithm for optimization, using the Deoptim package in R⁶⁹. The Hinshelwood and Eppley–Norberg approaches yielded similar curves (Supplementary Fig. 1).

Temperature as the primary driver of maximum division rates in *Prochlorococcus*

Our goal was to evaluate whether the observed decline in division rates at higher temperatures was primarily driven by temperature or by other covarying factors. The data were binned by 0.25 °C intervals of seawater temperature, and we analysed the 80th percentile division rate across each bin. The 80th percentile was chosen over the 99th percentile to

increase the sample size for statistical analysis while still focusing on the upper range of division rates. We used two complementary statistical models:

- (1) A generalized linear model was constructed using the glm function in R, incorporating polynomial terms for temperature, PAR, nitrate and phosphate. This allowed us to capture potential nonlinear relationships between these factors and division rates within a linear framework. Before the model fitting, all environmental factors were rescaled to have a mean of zero and a standard deviation of one to facilitate the comparison of their relative importance on division rates. To assess the robustness of model results, we applied a bootstrapping technique with 1,000 replicates, generating standard deviations for the model coefficients. Model fit was assessed using standard diagnostic plots and summary statistics.
- (2) A generalized additive model was constructed using the mgcv package in R, incorporating smooth terms (that is, estimated degree of freedom) for temperature, PAR, nitrogen (nitrate and nitrite) and phosphorus (phosphate) concentrations. A simulation-based test with 1,000 replicates indicated sufficient basis dimensions for all smooth terms, suggesting that the model adequately captured the complexity of the relationships. Model selection was performed using restricted maximum likelihood, and the basis dimension (k) was checked to ensure adequate model complexity.

Global climate change simulation

Ecosystem model. We used the Massachusetts Institute of Technology (MIT) marine ecosystem model (Darwin), including the cycling of carbon, nitrogen, phosphorus, silicon, iron and oxygen through inorganic, organic detritus and 50 plankton types, modified from previous studies^{45,70}. The model includes 31 phytoplankton types, analogues of the pico-cyanobacterium *Prochlorococcus*, *Synechococcus*, 2 sizes of green algae (picoeukaryotes), 5 sizes of coccolithophores, 5 diazotrophs, 9 diatoms and 8 mixotrophic dinoflagellates (Supplementary Fig. 2). To represent the wide range of phytoplankton sizes, we defined 14 size classes ranging from 0.6 µm to 104 µm ESD, evenly distributed on a logarithmic scale. The model also captures trophic interactions through 3 size classes of heterotrophic bacteria (0.4 µm to 0.9 µm ESD) that remineralize the organic matter and 16 size classes of zooplankton (4.5 µm to 1,636 µm ESD) that graze on prey following a Holling type II function⁷¹.

Phytoplankton growth parameters are allometrically defined with functional group specifics⁷². Growth rates are influenced by multiple potentially limiting nutrients (dissolved inorganic nitrogen, phosphate, iron and silicic acid) using Liebig's law of the minimum (growth limited by the scarcest resource) and parameterized with a Monod function (a mathematical relationship describing nutrient-limited growth). Nutrient half-saturation coefficients are allometrically assigned, favouring smaller phytoplankton with the highest nutrient affinity. Phytoplankton growth is also a function of spectral light and photoacclimation^{72,73} with functional groups showing distinct absorption patterns based on their specific pigment composition. Temperature affects all biological rates, including phytoplankton growth rates, zooplankton grazing rates and other loss rates. While these rates incorporate Q_{10} -based temperature dependencies, whose uncertainties and impacts on projections have been assessed in previous studies^{42,45}, our analysis shows that the choice of thermal response functions (that is, with or without thermal limits) represents a more significant source of uncertainty. This is particularly evident for *Prochlorococcus*, in which we evaluated two distinct thermal response curves: a conventional exponential function (solid blue curve; Supplementary Fig. 3) and a metabolic function incorporating thermal limits (dashed blue curve; Supplementary Fig. 3), both derived from in situ and laboratory studies

(Fig. 2a). For *Synechococcus*, we use an exponential thermal response curve (black curve; Supplementary Fig. 3) derived from in situ dilution experiments²⁷ and laboratory studies⁴². For all non-pico-cyanobacteria, we use exponential thermal growth functions (Supplementary Fig. 3 and parameters in Supplementary Table 4) derived from laboratory observations⁴⁵.

Climate model and simulation procedure. Our study integrates the biological and biogeochemical components of the Darwin ecosystem within an Earth system model of intermediate complexity, the MIT Integrated Global System Model (IGSM)^{74–76}. The IGSM couples the MIT general circulation model⁷⁷, a three-dimensional ocean circulation model at a coarse resolution configuration (2° by 2.5° horizontally, 22 vertical levels that range from 10 m at the surface to 500 m at depth)⁷⁶, with a simplified representation of the atmospheric dynamics, physics and chemistry, terrestrial water, energy and biogeochemical processes⁷⁸. The Darwin model is run in ‘offline’ mode using physical ocean fields (for example, circulation, mixing, salinity and temperature) from representative members of an ensemble of IGSM simulations. The ocean component of the IGSM shows a realistic climatology and year-to-year variability (for example, El Niño–Southern Oscillation) with frequency, seasonality, magnitude and patterns in general agreement with observations⁷⁵. As is typical with climate change studies, the IGSM performed a ‘control’ simulation in which greenhouse gas and aerosol concentrations were held constant at 1860 levels. This pre-industrial control shows interannual variability but lacks any long-term warming trends or circulation changes. In addition, the IGSM performed a transient simulation from 1860 to 2100 under observed pre-industrial changes in greenhouse gas and aerosol concentrations followed by two future greenhouse gas and aerosol emission scenarios, a moderate and high scenario similar to Intergovernmental Panel Climate Change RCP 4.5 and 8.5. These simulations have been previously described and evaluated in detail⁷⁵. Following the approach in a previous study⁴⁵, we conducted paired ecosystem model experiments (20 years each) to contrast pre-industrial and projected future ocean conditions (Extended Data Fig. 6). This capitalized on the significant differences in ocean physics between the pre-industrial control run of the IGSM and its end-of-century moderate and high warming scenarios. We initialized each simulation with nutrient and detritus fields from previous transient simulations⁷⁹, ensuring consistency with pre-industrial or future conditions. Plankton types were initialized at low abundances, and robust ecosystem structures were established within 3 years. Our results represent averages over the past 10 years of each simulation. This averaging mitigates the impact of interannual variability on the comparison between pre-industrial and future conditions.

Series of simulations. We perform a series of simulations varying both physical conditions and the thermal response function used for *Prochlorococcus* (Supplementary Table 4). We refer to simulations with constant 1860 greenhouse gas and aerosol concentrations (control run) as ‘pre-industrial’ and those based on projected end-of-century physical conditions as ‘2090–2100’. Simulations in which *Prochlorococcus* maximum division rates follow an exponential temperature function are termed ‘exponential’, while those using a metabolic function with an upper thermal limit are termed ‘metabolic’. Our initial set of six simulations (two paired experiments; Supplementary Table 5) are the ones discussed in the main text: ‘exponential’ pre-industrial, moderate and warming scenarios, and ‘metabolic’ pre-industrial, moderate and high warming scenarios. Phytoplankton distributions and production in pre-industrial simulations align well with real-world observations (Extended Data Figs. 7 and 8), as shown in previous studies^{45,70}. While the computational demands of this global three-dimensional ecosystem model preclude comprehensive parameter sensitivity analyses, we note that the projected changes between ‘pre-industrial’ and future climate simulations exceed the model’s interannual variability by an

order of magnitude (Supplementary Table 6). This, combined with the model’s demonstrated skill in reproducing present-day distributions, provides confidence in the robustness of our key findings.

To isolate the direct impact of temperature change on *Prochlorococcus*, we conducted two additional simulations. In these experiment, we maintained pre-industrial circulation patterns and nutrient concentrations to control for changes in nutrient supply, while allowing biological rates (including *Prochlorococcus* growth rate) to respond to projected end-of-century warming for both climate scenarios (Supplementary Table 5). In the main text, we compare the results of the 2090–2100 simulations to their paired pre-industrial counterparts (Figs. 3 and 4 and Extended Data Figs. 7 and 10).

Reporting summary

Further information on research design is available in the Nature Portfolio Reporting Summary linked to this article.

Data availability

All data used to support the findings of this study, including *Prochlorococcus* division rates, cell abundances, environmental variables and model outputs, are available via Zenodo at <https://doi.org/10.5281/zenodo.11043386> (ref. 80). This repository includes figure source data and processed datasets used for statistical analyses.

Code availability

Source code and workflow for the size-structured matrix population model are publicly available via GitHub at <https://github.com/seaflo-uw/mpm-workflow>. Darwin ecosystem model source code and parameters are available via Harvard Dataverse at <https://doi.org/10.7910/DVN/CGGMW2> and <https://doi.org/10.7910/DVN/WAG17U>. Code for the statistical analysis, thermal response modelling and figure generation are available via Zenodo at <https://doi.org/10.5281/zenodo.11043386> (ref. 80).

References

1. Cheng, L. et al. New record ocean temperatures and related climate indicators in 2023. *Adv. Atmos. Sci.* <https://doi.org/10.1007/s00376-024-3378-5> (2024).
2. Wang, G., Xie, S.-P., Huang, R. X. & Chen, C. Robust warming pattern of global subtropical oceans and its mechanism. *J. Clim.* **28**, 8574–8584 (2015).
3. Penn, J. L. & Deutsch, C. Avoiding ocean mass extinction from climate warming. *Science* **376**, 524–526 (2022).
4. Bopp, L. et al. Potential impact of climate change on marine export production. *Glob. Biogeochem. Cycles* **15**, 81–99 (2001).
5. Plattner, G.-K., Joos, F., Stocker, T. F. & Marchal, O. Feedback mechanisms and sensitivities of ocean carbon uptake under global warming. *Tellus B* **53**, 564–592 (2001).
6. Morán, X. A. G., López-Urrutia, Á., Calvo-Díaz, A. & Li, W. K. W. Increasing importance of small phytoplankton in a warmer ocean. *Glob. Change Biol.* **16**, 1137–1144 (2010).
7. Edwards, M. & Richardson, A. J. Impact of climate change on marine pelagic phenology and trophic mismatch. *Nature* **430**, 881–884 (2004).
8. Richardson, T. L. Mechanisms and pathways of small-phytoplankton export from the surface ocean. *Ann. Rev. Mar. Sci.* **11**, 57–74 (2019).
9. Marañón, E., Lorenzo, M. P., Cermeño, P. & Mourinho-Carballido, B. Nutrient limitation suppresses the temperature dependence of phytoplankton metabolic rates. *ISME J.* **12**, 1836–1845 (2018).
10. Thomas, M. K., Kremer, C. T., Klausmeier, C. A. & Litchman, E. A global pattern of thermal adaptation in marine phytoplankton. *Science* **338**, 1085–1088 (2012).
11. Partensky, F. & Garczarek, L. *Prochlorococcus*: advantages and limits of minimalism. *Ann. Rev. Mar. Sci.* **2**, 305–331 (2010).

12. Biller, S. J., Berube, P. M., Lindell, D. & Chisholm, S. W. *Prochlorococcus*: the structure and function of collective diversity. *Nat. Rev. Microbiol.* **13**, 13–27 (2015).
13. Martiny, A. C. et al. Marine phytoplankton resilience may moderate oligotrophic ecosystem responses and biogeochemical feedbacks to climate change. *Limnol. Oceanogr.* **67**, S378–S389 (2022).
14. Flombaum, P. et al. Present and future global distributions of the marine cyanobacteria *Prochlorococcus* and *Synechococcus*. *Proc. Natl Acad. Sci. USA* **110**, 9824–9829 (2013).
15. Laws, E. A. Evaluation of in situ phytoplankton growth rates: a synthesis of data from varied approaches. *Annu. Rev. Mar. Sci.* **5**, 247–268 (2013).
16. Swalwell, J. E., Ribalet, F. & Armbrust, E. V. SeaFlow: a novel underway flow-cytometer for continuous observations of phytoplankton in the ocean. *Limnol. Oceanogr. Methods* **9**, 466–477 (2011).
17. Ribalet, F. et al. SeaFlow data v1, high-resolution abundance, size and biomass of small phytoplankton in the North Pacific. *Sci. Data* **6**, 277 (2019).
18. Mattern, J. P. et al. A Bayesian approach to modeling phytoplankton population dynamics from size distribution time series. *PLoS Comput. Biol.* **18**, e1009733 (2022).
19. Hunter-Cevera, K. R. et al. Diel size distributions reveal seasonal growth dynamics of a coastal phytoplankton. *Proc. Natl Acad. Sci. USA* **111**, 9852–9857 (2014).
20. Ribalet, F. et al. Light-driven synchrony of *Prochlorococcus* growth and mortality in the subtropical Pacific gyre. *Proc. Natl Acad. Sci. USA* **112**, 8008–8012 (2015).
21. Hunter-Cevera, K. R. et al. Physiological and ecological drivers of early spring blooms of a coastal phytoplankton. *Science* **354**, 326–329 (2016).
22. Fowler, B. L. et al. Dynamics and functional diversity of the smallest phytoplankton on the Northeast US Shelf. *Proc. Natl Acad. Sci. USA* **117**, 12215–12221 (2020).
23. Grone, J. et al. A single *Prochlorococcus* ecotype dominates the tropical Bay of Bengal with ultradian growth. *Environ. Microbiol.* <https://doi.org/10.1111/1462-2920.16605> (2024).
24. Agawin, N. S. R. & Agustí, S. *Prochlorococcus* and *Synechococcus* cells in the central Atlantic Ocean: distribution, growth and mortality (grazing) rates. *Vie Milieu* **55**, 165–175 (2005).
25. Shalapyonok, A., Olson, R. J. & Shalapyonok, L. S. Ultradian growth in *Prochlorococcus* spp. *Appl. Environ. Microbiol.* **64**, 1066–1069 (1998).
26. Worden, A. & Binder, B. Application of dilution experiments for measuring growth and mortality rates among *Prochlorococcus* and *Synechococcus* populations in oligotrophic environments. *Aquat. Microb. Ecol.* **30**, 159–174 (2003).
27. Liu, K., Suzuki, K., Chen, B. & Liu, H. Are temperature sensitivities of *Prochlorococcus* and *Synechococcus* impacted by nutrient availability in the subtropical northwest Pacific? *Limnol. Oceanogr.* **66**, 639–651 (2021).
28. Jiang, S. et al. Variations in physiology and genomic function of *Prochlorococcus* across the eastern Indian Ocean. *J. Geophys. Res. Oceans* **128**, e2023JC019898 (2023).
29. Kuipers, B. R. & Witte, H. J. Prochlorophytes as secondary prey for heterotrophic nanoflagellates in the deep chlorophyll maximum layer of the (sub)tropical North Atlantic. *Mar. Ecol. Prog. Ser.* **204**, 53–63 (2000).
30. Liu, H., Nolla, H. A. & Campbell, L. *Prochlorococcus* growth rate and contribution to primary production in the equatorial and subtropical North Pacific Ocean. *Aquat. Microb. Ecol.* **12**, 39–47 (1997).
31. Landry, M. R. et al. Microbial community biomass, production and grazing along 110° E in the eastern Indian Ocean. *Deep Sea Res.* **202**, 105134 (2022).
32. Chen, B. et al. Close coupling between phytoplankton growth and microzooplankton grazing in the western South China Sea. *Limnol. Oceanogr.* **54**, 1084–1097 (2009).
33. Chen, M., Liu, H. & Li, H. Effect of mesozooplankton feeding selectivity on the dynamics of algae in presence of intermediate grazers—a laboratory simulation. *Mar. Ecol. Prog. Ser.* **486**, 47–58 (2013).
34. Brown, S. L. et al. Picophytoplankton dynamics and production in the Arabian Sea during the 1995 Southwest Monsoon. *Deep Sea Res.* **46**, 1745–1768 (1999).
35. Reckermann, M. & Veldhuis, M. Trophic interactions between picophytoplankton and micro- and nanozooplankton in the western Arabian Sea during the NE monsoon 1993. *Aquat. Microb. Ecol.* **12**, 263–273 (1997).
36. Casey, J. R., Lomas, M. W., Mandecki, J. & Walker, D. E. *Prochlorococcus* contributes to new production in the Sargasso Sea deep chlorophyll maximum. *Geophys. Res. Lett.* **34**, L10604 (2007).
37. Johnson, Z. I. et al. Niche partitioning among *Prochlorococcus* ecotypes along ocean-scale environmental gradients. *Science* **311**, 1737–1740 (2006).
38. Biller, S. J. et al. Environmental and taxonomic drivers of bacterial extracellular vesicle production in marine ecosystems. *Appl. Environ. Microbiol.* **89**, e00594-23 (2023).
39. Zinser, E. R. et al. Influence of light and temperature on *Prochlorococcus* ecotype distributions in the Atlantic Ocean. *Limnol. Oceanogr.* **52**, 2205–2220 (2007).
40. Smith, A. N. et al. Comparing *Prochlorococcus* temperature niches in the lab and across ocean basins. *Limnol. Oceanogr.* **66**, 2632–2647 (2021).
41. Kremer, C. T., Thomas, M. K. & Litchman, E. Temperature- and size-scaling of phytoplankton population growth rates: reconciling the Eppley curve and the metabolic theory of ecology. *Limnol. Oceanogr.* **62**, 1658–1670 (2017).
42. Anderson, S. I., Barton, A. D., Clayton, S., Dutkiewicz, S. & Rynearson, T. A. Marine phytoplankton functional types exhibit diverse responses to thermal change. *Nat. Commun.* **12**, 6413 (2021).
43. Strauss, J. et al. The Bay of Bengal exposes abundant photosynthetic picoplankton and newfound diversity along salinity-driven gradients. *Environ. Microbiol.* **25**, 2118–2141 (2023).
44. Follows, M. J. & Dutkiewicz, S. Modeling diverse communities of marine microbes. *Annu. Rev. Mar. Sci.* **3**, 427–451 (2011).
45. Anderson, S. I. et al. Phytoplankton thermal trait parameterization alters community structure and biogeochemical processes in a modeled ocean. *Glob. Change Biol.* **30**, e17093 (2024).
46. Six, C., Ratin, M., Marie, D. & Corre, E. Marine *Synechococcus* picocyanobacteria: light utilization across latitudes. *Proc. Natl Acad. Sci. USA* **118**, e2111300118 (2021).
47. Barton, S. et al. Comparative experimental evolution reveals species-specific idiosyncrasies in marine phytoplankton adaptation to warming. *Glob. Change Biol.* **29**, 5261–5275 (2023).
48. Thomas, M. K. et al. Temperature–nutrient interactions exacerbate sensitivity to warming in phytoplankton. *Glob. Change Biol.* **23**, 3269–3280 (2017).
49. Labban, A., Shibl, A. A., Calleja, M. L., Hong, P.-Y. & Morán, X. A. G. Growth dynamics and transcriptional responses of a Red Sea *Prochlorococcus* strain to varying temperatures. *Environ. Microbiol.* **25**, 1007–1021 (2023).
50. Alonso-Sáez, L. et al. Transcriptional mechanisms of thermal acclimation in *Prochlorococcus*. *mBio* **14**, e03425-22 (2023).
51. Schiksnis, C. et al. Proteomics analysis reveals differential acclimation of coastal and oceanic *Synechococcus* to climate warming and iron limitation. *Front. Microbiol.* **15**, 1323499 (2024).

52. Dedman, C. J., Barton, S., Fournier, M. & Rickaby, R. E. M. Shotgun proteomics reveals temperature-dependent regulation of major nutrient metabolism in coastal *Synechococcus* sp. WH5701. *Algal Res.* **75**, 103279 (2023).
53. Britten, G. L. & Sibert, E. C. Enhanced fish production during a period of extreme global warmth. *Nat. Commun.* **11**, 5636 (2020).
54. Dutkiewicz, S., Boyd, P. W. & Riebesell, U. Exploring biogeochemical and ecological redundancy in phytoplankton communities in the global ocean. *Glob. Change Biol.* **27**, 1196–1213 (2021).
55. Archibald, K., Dutkiewicz, S., Laufkötter, C. & Moeller, H. V. Thermal responses in global marine planktonic food webs are mediated by temperature effects on metabolism. *J. Geophys. Res.* <https://doi.org/10.1029/2022JC018932> (2022).
56. Atkinson, A. et al. Steeper size spectra with decreasing phytoplankton biomass indicate strong trophic amplification and future fish declines. *Nat. Commun.* **15**, 381 (2024).
57. Braakman, R., Follows, M. J. & Chisholm, S. W. Metabolic evolution and the self-organization of ecosystems. *Proc. Natl Acad. Sci. USA* **114**, E3091–E3100 (2017).
58. Becker, J. W., Hogle, S. L., Rosendo, K. & Chisholm, S. W. Co-culture and biogeography of *Prochlorococcus* and SAR11. *ISME J.* **13**, 1506–1519 (2019).
59. Azam, F. & Malfatti, F. Microbial structuring of marine ecosystems. *Nat. Rev. Microbiol.* **5**, 782–791 (2007).
60. Ashkezari, M. D. et al. Simons Collaborative Marine Atlas Project (Simons CMAP): an open-source portal to share, visualize, and analyze ocean data. *Limnol. Oceanogr. Methods* **19**, 488–496 (2021).
61. Sosik, H. M., Olson, R. J., Neubert, M. G., Shalapyonok, A. & Solow, A. R. Growth rates of coastal phytoplankton from time-series measurements with a submersible flow cytometer. *Limnol. Oceanogr.* **48**, 1756–1765 (2003).
62. Hamilton, M. et al. Dynamics of *Teleaulax*-like cryptophytes during the decline of a red water bloom in the Columbia River Estuary. *J. Plankton Res.* **39**, 589–599 (2017).
63. Gelman, A. & Rubin, D. B. Inference from iterative simulation using multiple sequences. *Stat. Sci.* **7**, 457–472 (1992).
64. Jones, C., Clayton, S., Ribalet, F., Armbrust, E. V. & Harchaoui, Z. A kernel-based change detection method to map shifts in phytoplankton communities measured by flow cytometry. *Methods Ecol. Evol.* **12**, 1687–1698 (2021).
65. Aumont, O., Ethé, C., Tagliabue, A., Bopp, L. & Gehlen, M. PISCES-v2: an ocean biogeochemical model for carbon and ecosystem studies. *Geosci. Model Dev.* **8**, 2465–2513 (2015).
66. Global Ocean Biogeochemistry Analysis and Forecast. *E.U. Copernicus Marine Service Information (CMEMS)* <https://doi.org/10.48670/moi-00015> (2021).
67. Grimaud, G. M., Mairet, F., Sciandra, A. & Bernard, O. Modeling the temperature effect on the specific growth rate of phytoplankton: a review. *Rev. Environ. Sci. Biotechnol.* **16**, 625–645 (2017).
68. Bissinger, J. E., Montagnes, D. J. S., Sharples, J. & Atkinson, D. Predicting marine phytoplankton maximum growth rates from temperature: improving on the Eppley curve using quantile regression. *Limnol. Oceanogr.* **53**, 487–493 (2008).
69. Mullen, K. M., Ardia, D., Gil, D. L., Windover, D. & Cline, J. DEoptim: an R package for global optimization by differential evolution. *J. Stat. Softw.* **40**, 1–26 (2011).
70. Dutkiewicz, S. et al. Multiple biotic interactions establish phytoplankton community structure across environmental gradients. *Limnol. Oceanogr.* **69**, 1086–1100 (2024).
71. Holling, C. S. The functional response of predators to prey density and its role in mimicry and population regulation. *Mem. Entomol. Soc. Can.* **97**, 5–60 (1965).
72. Dutkiewicz, S. et al. Dimensions of marine phytoplankton diversity. *Biogeosciences* **17**, 609–634 (2020).
73. Dutkiewicz, S. et al. Capturing optically important constituents and properties in a marine biogeochemical and ecosystem model. *Biogeosciences* **12**, 4447–4481 (2015).
74. Sokolov, A. P. et al. *MIT Integrated Global System Model (IGSM) Version 2: Model Description and Baseline Evaluation* (2005); <https://dspace.mit.edu/handle/1721.1/29789>
75. Monier, E., Scott, J. R., Sokolov, A. P., Forest, C. E. & Schlosser, C. A. An integrated assessment modeling framework for uncertainty studies in global and regional climate change: the MIT IGSM-CAM (version 1.0). *Geosci. Model Dev.* **6**, 2063–2085 (2013).
76. Monier, E. et al. Toward a consistent modeling framework to assess multi-sectoral climate impacts. *Nat. Commun.* **9**, 660 (2018).
77. Marshall, J., Adcroft, A., Hill, C., Perelman, L. & Heisey, C. A finite-volume, incompressible Navier Stokes model for studies of the ocean on parallel computers. *J. Geophys. Res. Oceans* **102**, 5753–5766 (1997).
78. Sokolov, A. et al. Description and evaluation of the MIT Earth System Model (MESM). *J. Adv. Model. Earth Syst.* **10**, 1759–1789 (2018).
79. Henson, S. A., Cael, B. B., Allen, S. R. & Dutkiewicz, S. Future phytoplankton diversity in a changing climate. *Nat. Commun.* **12**, 5372 (2021).
80. Ribalet, F., Dutkiewicz, S., Monier, E. & Armbrust, E. V. Future ocean warming threatens key photosynthetic microbes. *Zenodo* <https://doi.org/10.5281/zenodo.11043386> (2024).

Acknowledgements

We thank the officers, crew and chief scientists aboard the research vessel Thomas G. Thompson for their assistance during the cruises. We thank K. Cain for operating SeaFlow, A. Hynes for processing SeaFlow data and C. Berthiaume for code development. This study was supported by grants from the Simons Foundation (574495 to F.R., 329108 to E.V.A., 549931 to S.D.) and other government, foundation and industry funders of the MIT Center for Sustainability Science and Strategy (for a complete list of funding sources, see <https://globalchange.mit.edu/sponsors/current>).

Author contributions

Conceptualization: F.R., S.D., E.V.A. and E.M. Methodology: F.R., S.D. and E.M. Investigation: F.R. Visualization: F.R. and S.D. Funding acquisition: F.R., S.D. and E.V.A. Project administration: F.R. Writing—original draft: F.R. Writing—review and editing: F.R., S.D., E.V.A. and E.M.

Competing interests

The authors declare no competing interests.

Additional information

Extended data is available for this paper at <https://doi.org/10.1038/s41564-025-02106-4>.

Supplementary information The online version contains supplementary material available at <https://doi.org/10.1038/s41564-025-02106-4>.

Correspondence and requests for materials should be addressed to François Ribalet.

Peer review information *Nature Microbiology* thanks Laurent Bopp and the other, anonymous, reviewer(s) for their contribution to the peer review of this work. Peer reviewer reports are available.

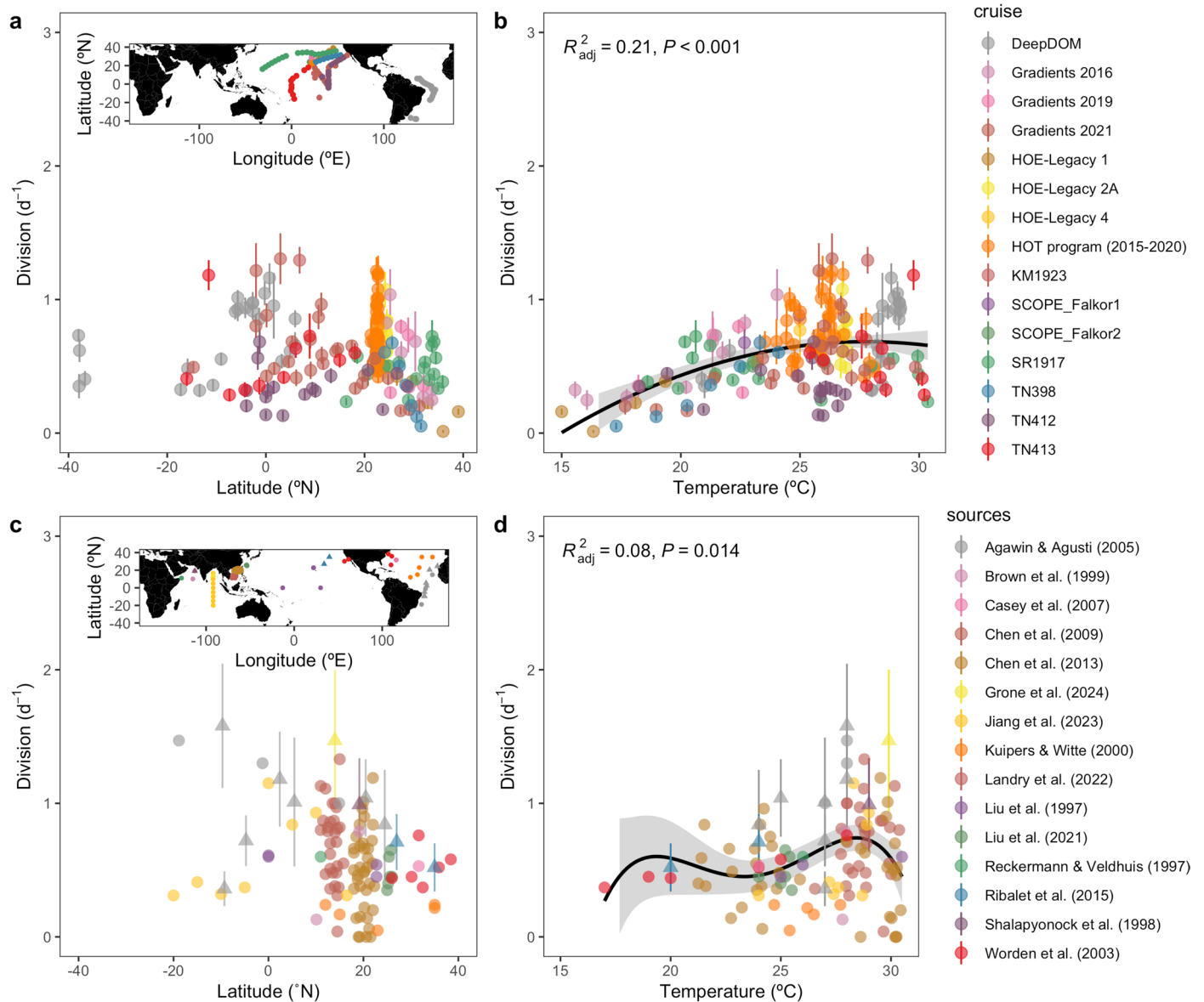
Reprints and permissions information is available at www.nature.com/reprints.

Publisher's note Springer Nature remains neutral with regard to jurisdictional claims in published maps and institutional affiliations.

Open Access This article is licensed under a Creative Commons Attribution-NonCommercial-NoDerivatives 4.0 International License, which permits any non-commercial use, sharing, distribution and reproduction in any medium or format, as long as you give appropriate credit to the original author(s) and the source, provide a link to the Creative Commons licence, and indicate if you modified the licensed material. You do not have permission under this licence to share

adapted material derived from this article or parts of it. The images or other third party material in this article are included in the article's Creative Commons licence, unless indicated otherwise in a credit line to the material. If material is not included in the article's Creative Commons licence and your intended use is not permitted by statutory regulation or exceeds the permitted use, you will need to obtain permission directly from the copyright holder. To view a copy of this licence, visit <http://creativecommons.org/licenses/by-nc-nd/4.0/>.

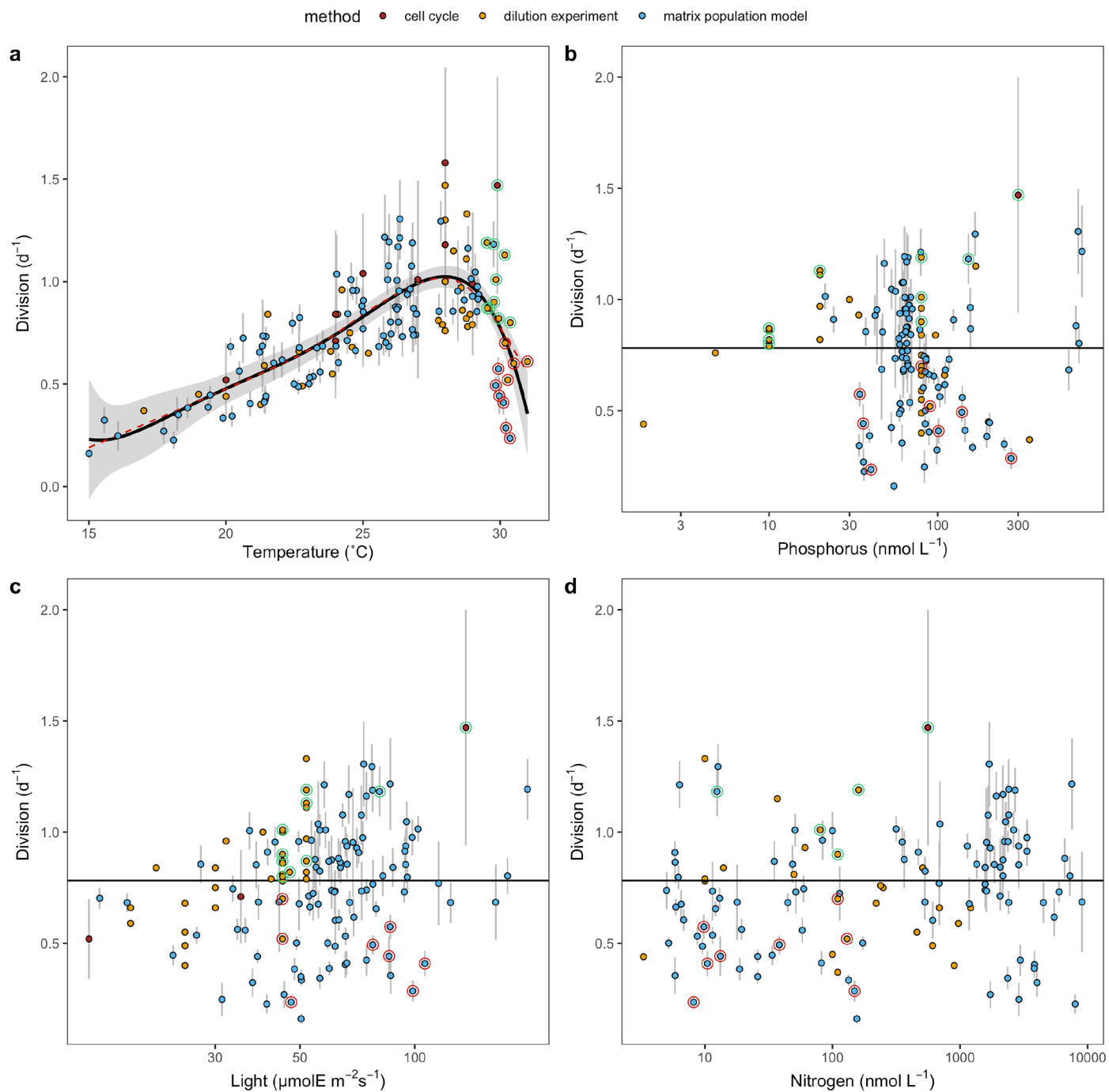
© The Author(s) 2025, corrected publication 2025



Extended Data Fig. 1 | Global patterns in *Prochlorococcus* division rates (d^{-1}) in surface waters.

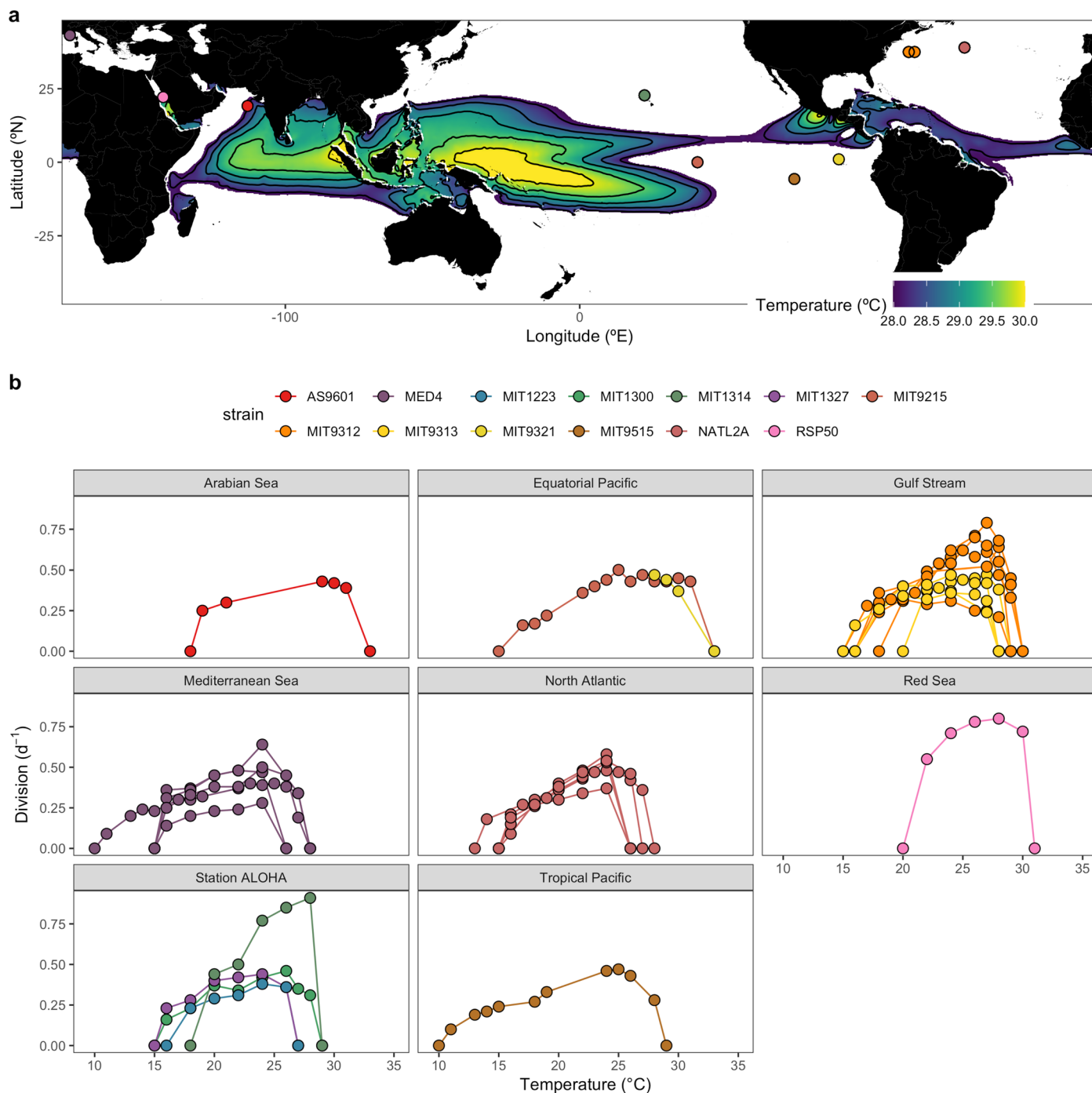
a, Geographic distribution of daily division rates derived from the matrix population model ($n = 180$ independent samples). **b**, Relationship between division rates derived from the matrix population model and seawater temperature (°C). **c**, Geographic distribution of daily division rates derived from data compilations of dilution experiments (circles, $n = 103$ independent samples)^{24,26-36} and cell cycle analysis (triangles, $n = 11$ independent samples)^{20,23-25}. **d**, Relationship between division rates derived from dilution experiments (circles) and cell cycle analysis (triangles) and seawater temperature (°C). The inset map in **a** and **c** shows the geographical distribution of sample

locations. Statistical relationships in **b** and **d** were assessed using ordinary least squares regression with two-sided tests ($\alpha = 0.01$). The black line in **b** shows a second-order polynomial regression model fit ($P = 3.349 \times 10^{-10}$); **d** shows a fourth-order polynomial regression fit ($P = 0.014$). No adjustments for multiple comparisons were applied. Error bars in **a** and **b** represent standard deviation of the 2000 Markov Chain Monte Carlo iterations used to infer division rates with the matrix population model. Error bars in **c** and **d** represent standard deviation in estimating duration of S phase in cell cycle method. Uncertainty estimates were not reported for dilution experiments.



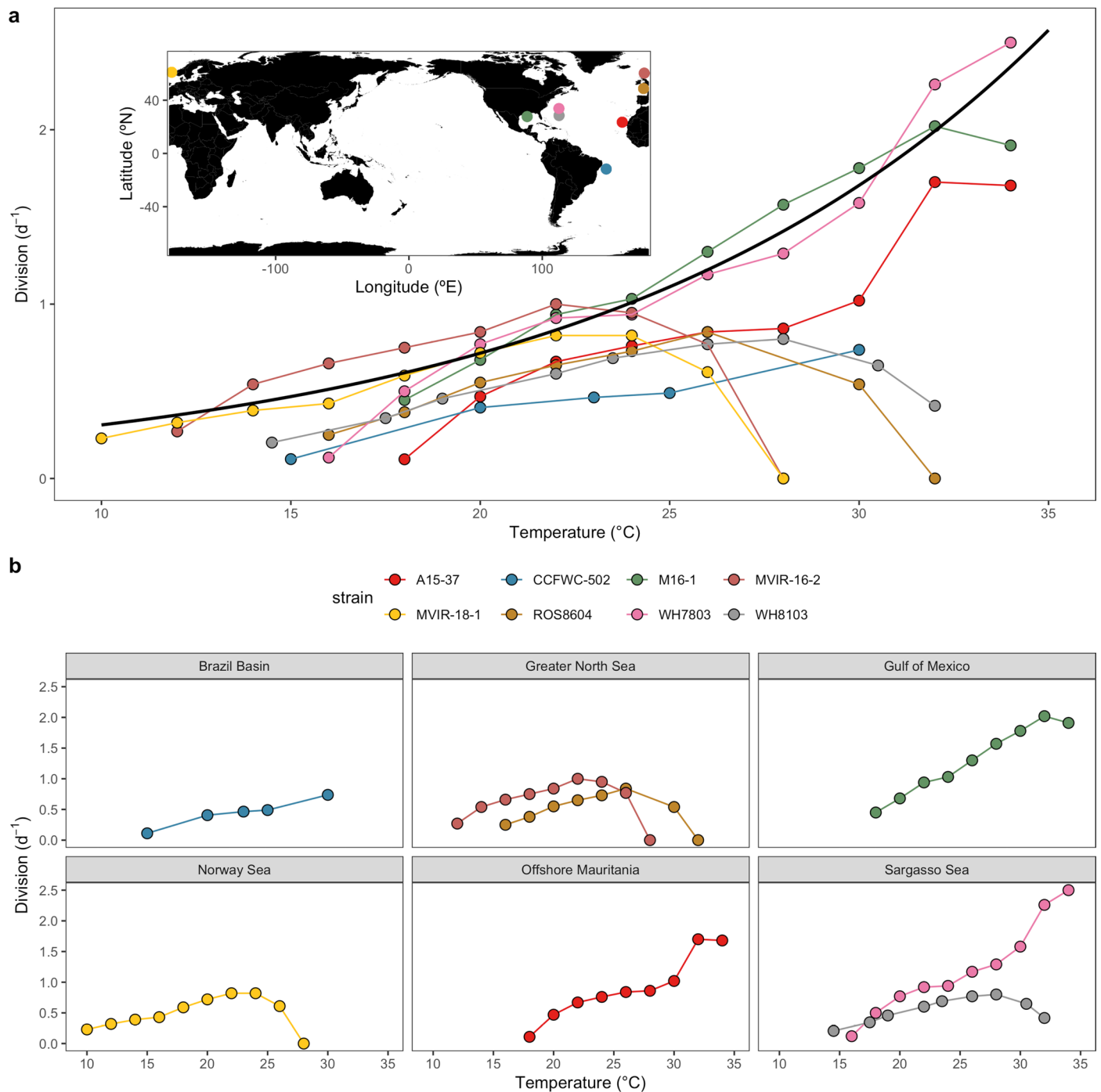
Extended Data Fig. 2 | Relationship between *Prochlorococcus maximum* division rates (d^{-1}) and environmental variables. **a, Data were binned by 0.25°C intervals of seawater temperature, and the 80th percentile division rate was calculated for each bin. The lines represent a fitted generalized linear model (black) with standard error (grey shading) and generalized additive model (dotted red) (see Supplementary Table 3), illustrating the relationships between maximum division rates and seawater temperature ($^{\circ}\text{C}$). **b-d**, Relationships between division rates derived from all three methods (matrix population model,**

dilution experiments, and cell cycle analysis) and phosphorus concentration (nmol L^{-1}) (**b**), light ($\mu\text{mol photons m}^{-2}\text{s}^{-1}$) (**c**), and nitrogen concentration (nmol L^{-1}) (**d**). Error bars represent standard deviation of the 2000 Markov Chain Monte Carlo iterations used to infer division rates with the matrix population model, and standard deviation in estimating duration of S phase in cell cycle method. Uncertainty estimates were not reported for dilution experiments. Red and green circles highlight division rates observed at the highest temperatures that fall below (red) or above (green) the regression line in panel **a**.



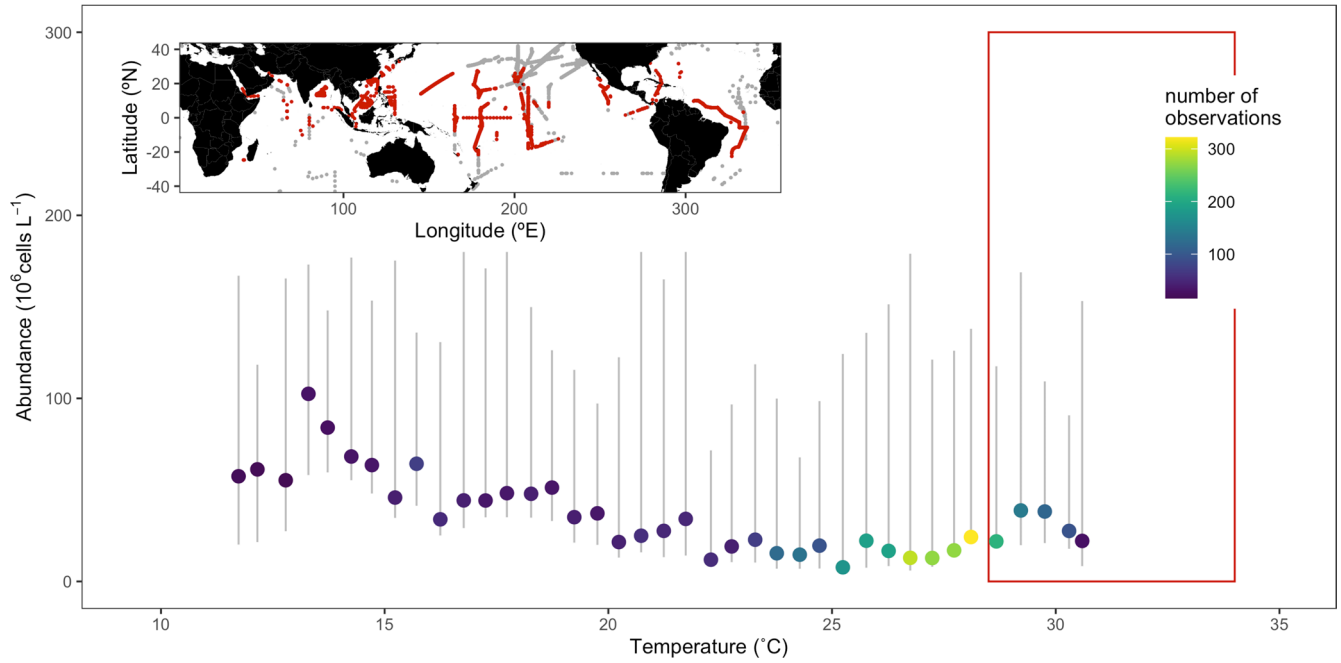
Extended Data Fig. 3 | Temperature response functions for *Prochlorococcus* across different strains. a, Map of *Prochlorococcus* strain isolation locations, colored by strains. The colored region represent areas where the climatological annual mean sea surface temperature exceeds 28 °C. **b,** Temperature response

curves (division rate vs. temperature) for each *Prochlorococcus* strain, grouped by isolation region. Points represent measured division rates under laboratory conditions from data compilations^{37–39}.



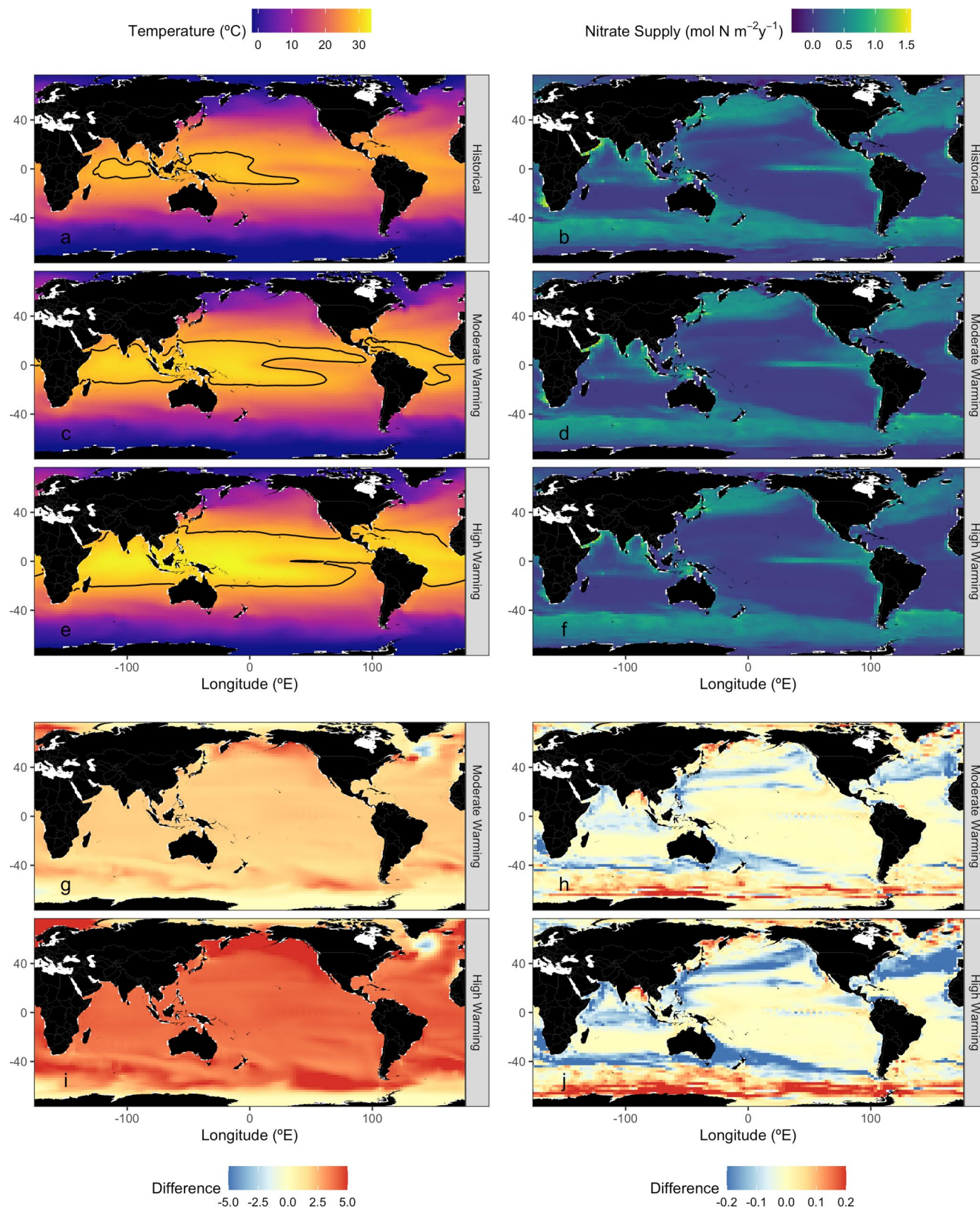
Extended Data Fig. 4 | Temperature response functions for *Synechococcus* across different strains. a, Map of *Synechococcus* isolation locations, colored by strain. The black line represents the fit of an Eppley exponential thermal response model (as described in Grimaud et al.⁶⁷) to the maxima division rates

observed for a given temperature across all strains. **b**, Temperature response curves (division rate vs. temperature) for each strain, grouped by isolation region. Points represent measured division rates under laboratory conditions from data compilations^{42,46}.



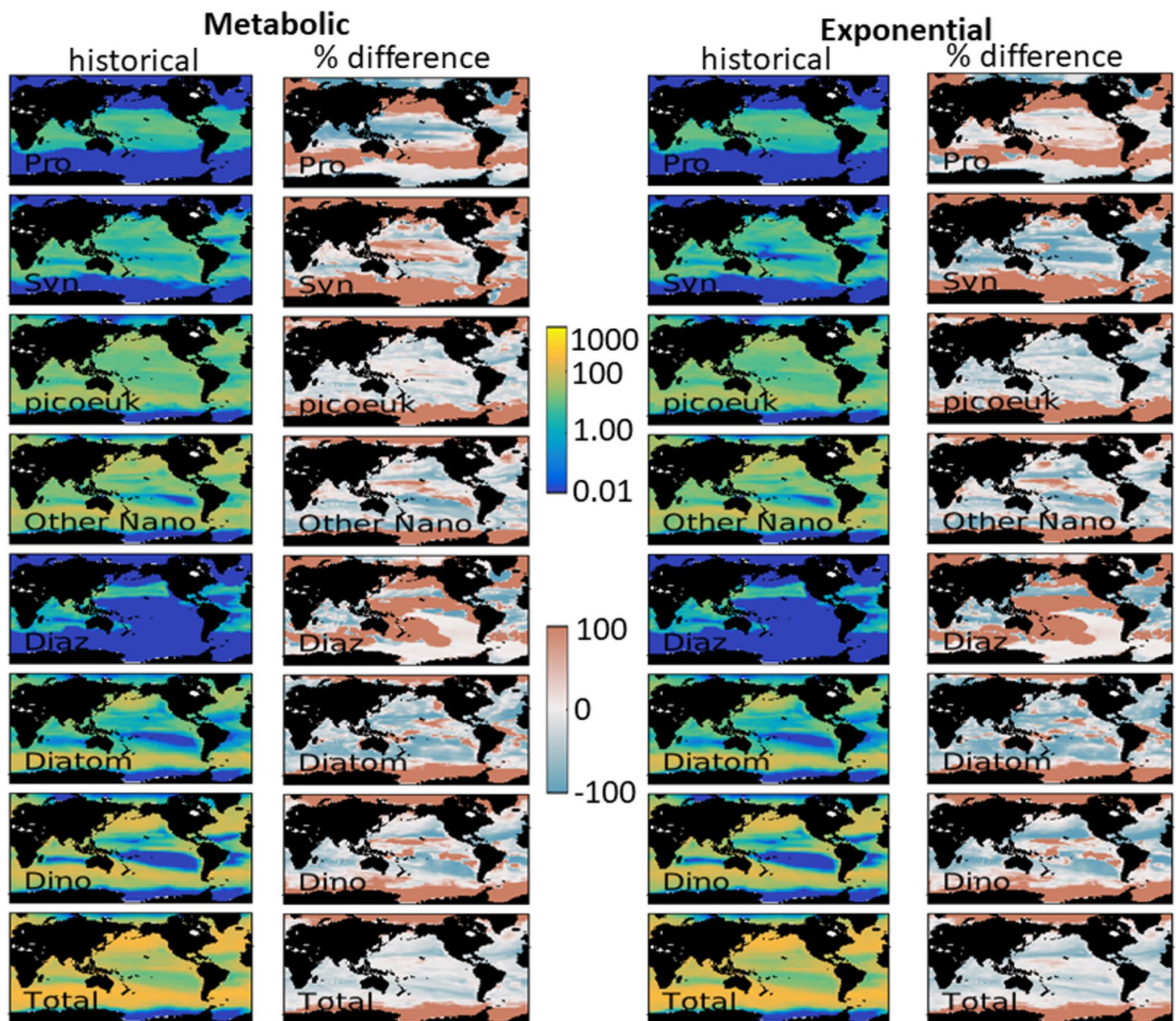
Extended Data Fig. 5 | Temperature-dependent responses of *Synechococcus* abundances. *Synechococcus* abundances measured by SeaFlow and compiled datasets^{14,23,43}, as a function of temperature (°C), with color scale coding representing the number of observations. The data were binned by 0.25 °C intervals of seawater temperature, and the 80th percentile abundance was

calculated for each bin. Error bars show the 5th and 95th percentiles within the top 80% subset. The red box highlights the observed detrimental effects of warm temperatures on *Prochlorococcus* (> 28 °C). The inset map shows the geographical distribution of sample locations, with samples collected in water above 28 °C indicated in red.



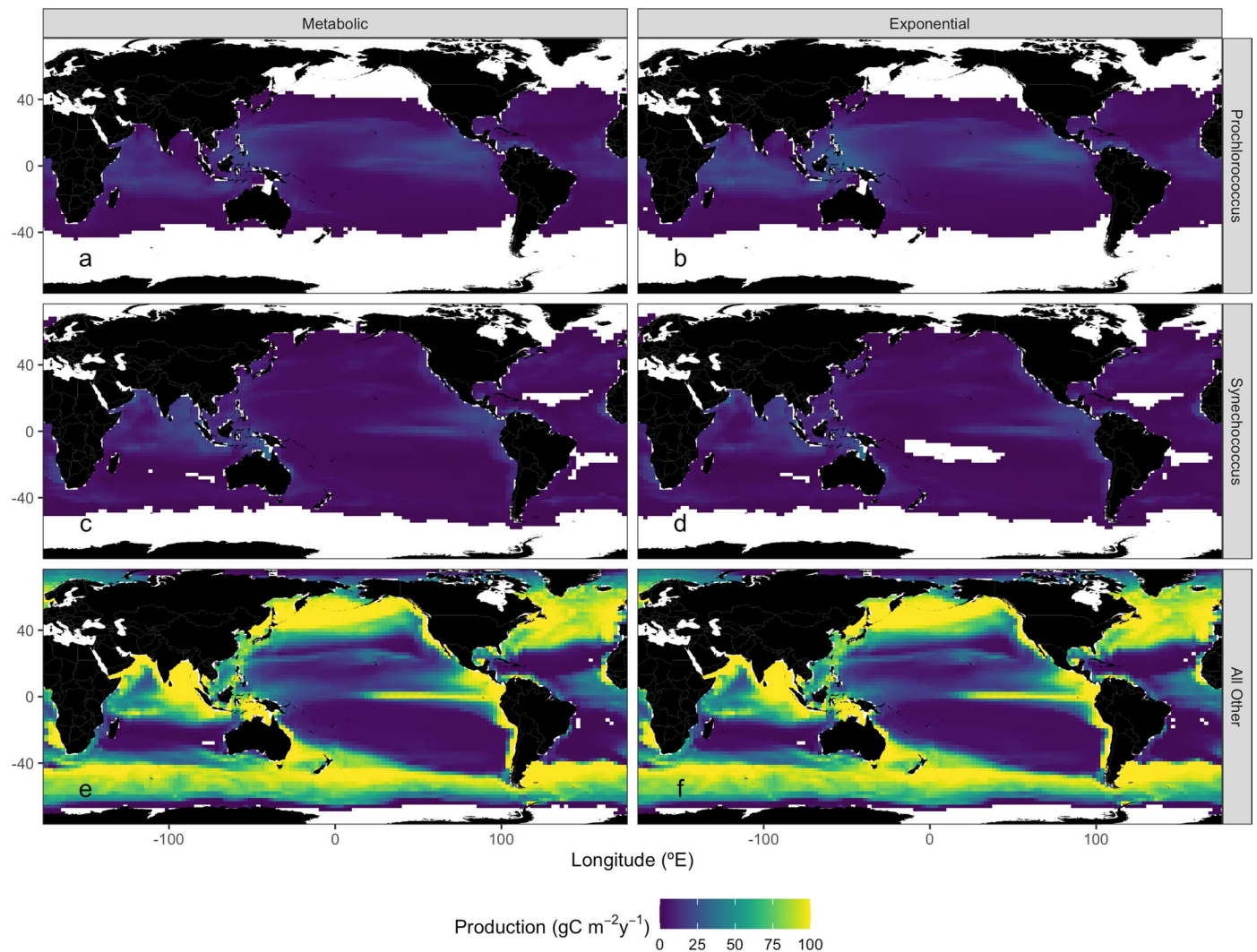
Extended Data Fig. 6 | Modelled Environmental Variables Affecting *Prochlorococcus* Division Rate. Temperature and nutrient supply to the sunlit layers of the ocean are two key environmental factors influencing phytoplankton division rates. **a, c, e, g, i.** Temperature ($^{\circ}\text{C}$) in the upper 10 m for pre-industrial conditions (**a**) and the 10-year average from 2090-2100 under moderate (**c**) and high warming scenario (**e**), with a black contour indicating 28°C , a critical temperature for *Prochlorococcus*. Change in temperature ($^{\circ}\text{C}$) between these periods (positive = warming) (**g, i**). **b, d, f, h, j.** Physical supply rate of nitrate to

the upper 50 m ($\text{mol N m}^{-2} \text{y}^{-1}$) under pre-industrial conditions (**b**) and future scenarios (**d, f**). Change in supply rate between these periods (negative = decreasing supply rate in the future) (**h, j**). Nutrient supply rates include lateral and vertical advection and mixing (metabolic simulations). In the tropics and subtropics, macronutrient supply decreases due to increased stratification and circulation changes. In polar regions, reduced sea ice leads to deeper mixing and increased nutrient supply. In some temperate waters, increased biological rates and nutrient trapping allow for higher supply rates in the future.



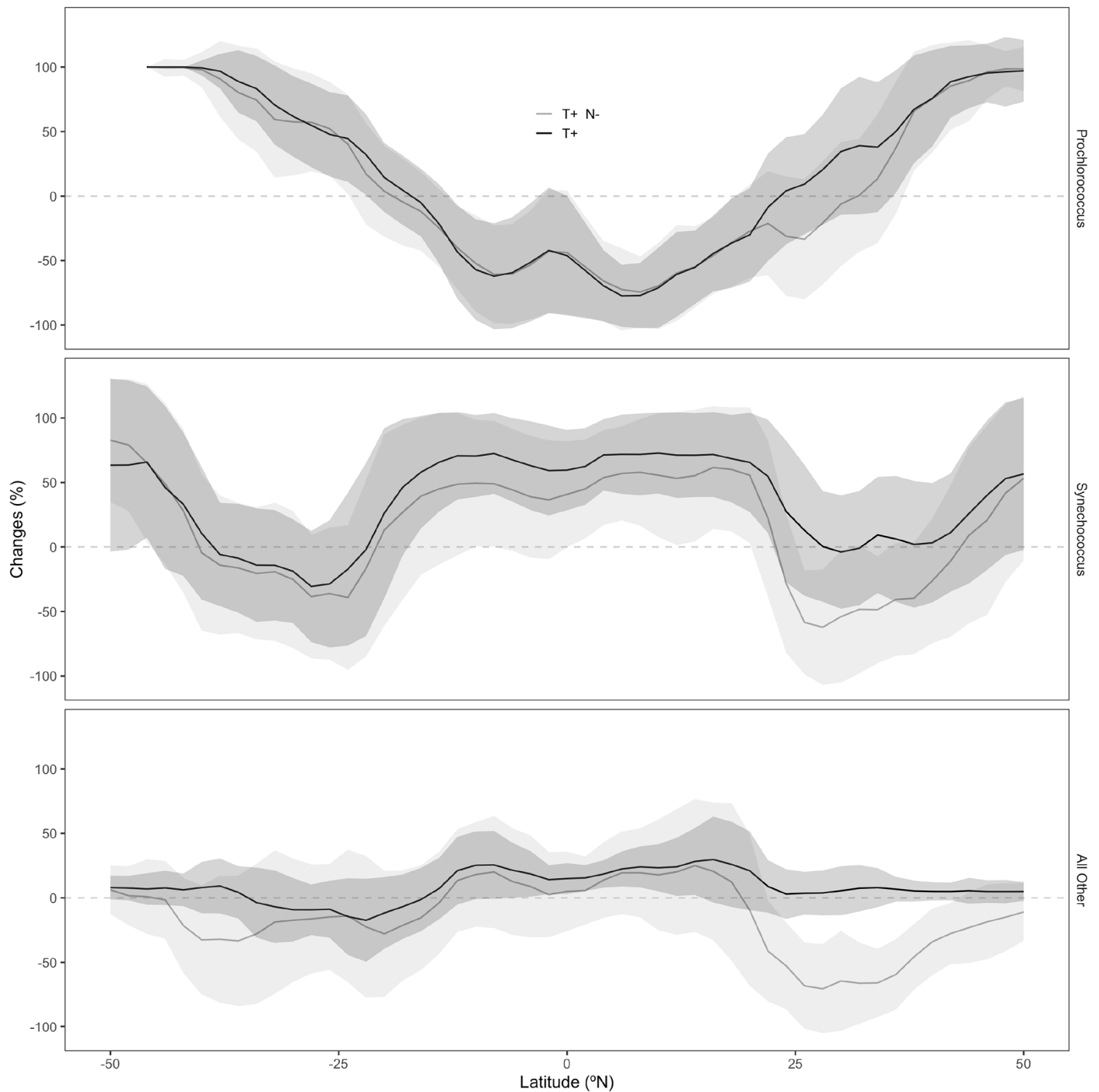
Extended Data Fig. 7 | Projected Impacts of Climate Change on Phytoplankton Biomass between pre-industrial (1860) and future (2090-2100) conditions, based on alterations in temperature, nutrient supply, mixing, and ocean circulation anticipated under high warming scenario. Depth-integrated biomass of different phytoplankton types under pre-industrial conditions and percent difference from a high warming scenario for the period 2090-2100. Two different thermal response functions for *Prochlorococcus* are used: metabolic (columns 1 and 2) and exponential (columns 3 and 4). Pre-industrial biomass

(10-year mean, mgC m^{-3}) for various phytoplankton types and total biomass, using the metabolic (column 1) and exponential (column 3) functions for *Prochlorococcus*. Percent change in biomass between pre-industrial and future conditions under a high warming scenario, using the metabolic (column 2) and exponential (column 4) functions. Positive values indicate an increase in biomass in the future scenario. Increases in biomass for specific phytoplankton types suggest niche shifts, with some groups outcompeting others.



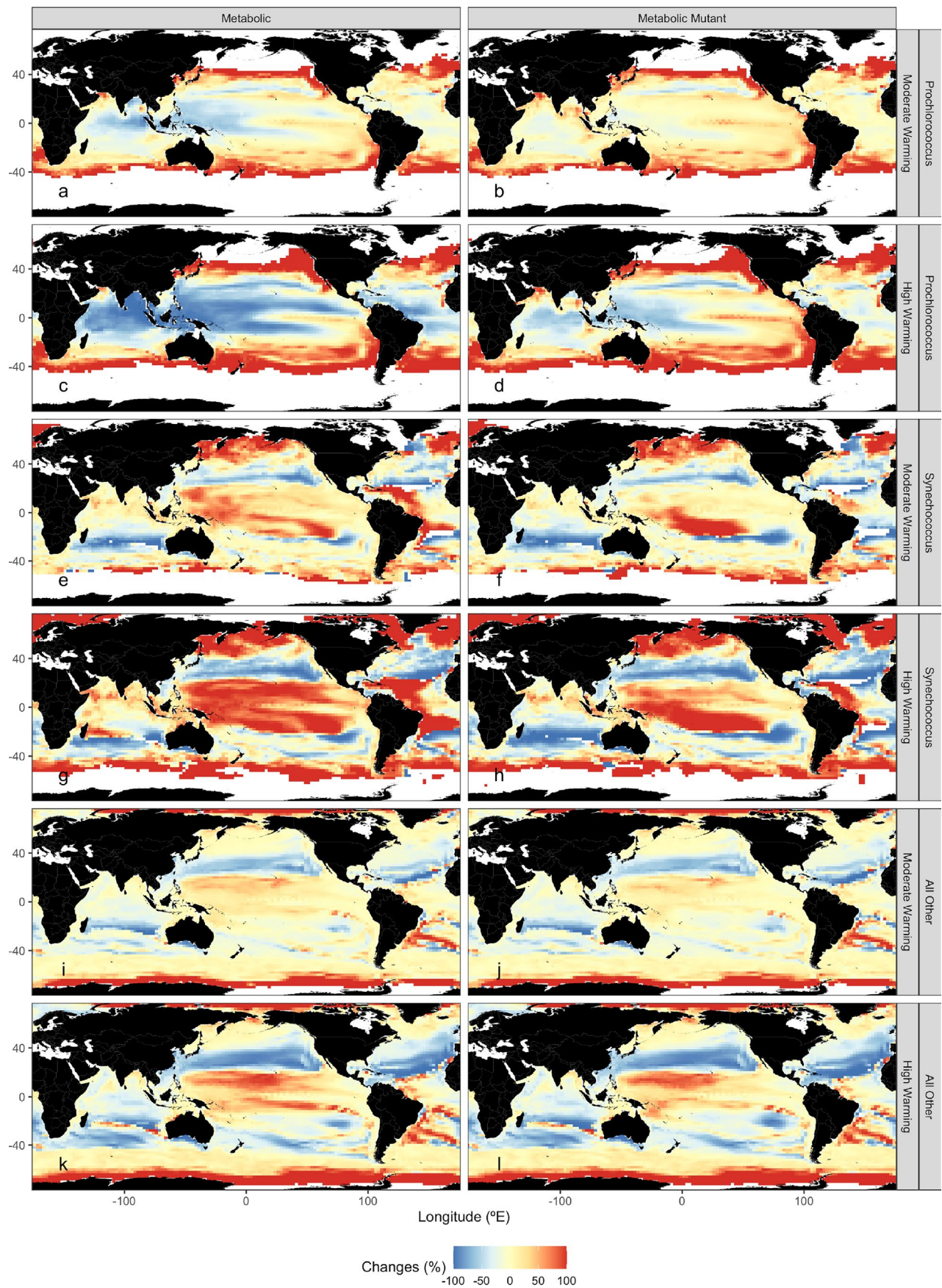
Extended Data Fig. 8 | Modelled Biomass Production. We compare modelled biomass production ($\text{gC m}^{-2}\text{y}^{-1}$) under pre-industrial conditions using either metabolic (left column) or exponential (right column) thermal response functions for *Prochlorococcus*. **a, b**, *Prochlorococcus* production, **c, d**, *Synechococcus* production, and **e, f**, production by all other phytoplankton. The color scale in

panels e and f is supersaturated to enhance visibility of patterns in panels a-d. Note that maximum production rates in some region exceed $100 \text{ gC m}^{-2}\text{y}^{-1}$. The percentage change in production between pre-industrial and future conditions is shown in Fig. 3.



Extended Data Fig. 9 | Projected latitudinal changes in annual phytoplankton biomass production between pre-industrial (1860) and future (2090-2100) conditions, based on alterations in temperature, nutrient supply, mixing, and ocean circulation anticipated under a high warming scenario. Latitudinal change (%) in depth-integrated biomass production for *Prochlorococcus*, *Synechococcus* and the combined total of all other phytoplankton. Results are

based on the metabolic thermal response function for *Prochlorococcus*. Grey line (T + N-) represents changes due to the combination of temperature and nutrient shifts between pre-industrial and future conditions. Black line (T +) represents changes due solely to temperature shifts, with circulation and nutrient concentrations held at pre-industrial levels (Methods and Supplementary Table 5). Shading represents the longitudinal variation from the mean (SD).



Extended Data Fig. 10 | See next page for caption.

Extended Data Fig. 10 | Impacts of a hypothetical warm-adapted *Prochlorococcus* strain on projected biomass production. Percentage change in depth-integrated annual biomass production for *Prochlorococcus* (a-d), *Synechococcus* (e-h), and all other phytoplankton (i-l) comparing the standard metabolic reaction model (left column) with a warm-adapted variant

(right column) for *Prochlorococcus*. Both projections use the same future climate scenarios (2090-2100) and pre-industrial baseline (1860) as Fig. 3. White areas indicate that the phytoplankton type does not exist in those regions in either pre-industrially or by end of century. Values of 100% increase indicates an expansion in the geographical range.

Reporting Summary

Nature Portfolio wishes to improve the reproducibility of the work that we publish. This form provides structure for consistency and transparency in reporting. For further information on Nature Portfolio policies, see our [Editorial Policies](#) and the [Editorial Policy Checklist](#).

Statistics

For all statistical analyses, confirm that the following items are present in the figure legend, table legend, main text, or Methods section.

n/a | Confirmed

- | | | |
|-------------------------------------|-------------------------------------|--|
| <input type="checkbox"/> | <input checked="" type="checkbox"/> | The exact sample size (n) for each experimental group/condition, given as a discrete number and unit of measurement |
| <input type="checkbox"/> | <input checked="" type="checkbox"/> | A statement on whether measurements were taken from distinct samples or whether the same sample was measured repeatedly |
| <input type="checkbox"/> | <input checked="" type="checkbox"/> | The statistical test(s) used AND whether they are one- or two-sided
<i>Only common tests should be described solely by name; describe more complex techniques in the Methods section.</i> |
| <input type="checkbox"/> | <input checked="" type="checkbox"/> | A description of all covariates tested |
| <input type="checkbox"/> | <input checked="" type="checkbox"/> | A description of any assumptions or corrections, such as tests of normality and adjustment for multiple comparisons |
| <input type="checkbox"/> | <input checked="" type="checkbox"/> | A full description of the statistical parameters including central tendency (e.g. means) or other basic estimates (e.g. regression coefficient) AND variation (e.g. standard deviation) or associated estimates of uncertainty (e.g. confidence intervals) |
| <input type="checkbox"/> | <input checked="" type="checkbox"/> | For null hypothesis testing, the test statistic (e.g. F , t , r) with confidence intervals, effect sizes, degrees of freedom and P value noted
<i>Give P values as exact values whenever suitable.</i> |
| <input type="checkbox"/> | <input checked="" type="checkbox"/> | For Bayesian analysis, information on the choice of priors and Markov chain Monte Carlo settings |
| <input checked="" type="checkbox"/> | <input type="checkbox"/> | For hierarchical and complex designs, identification of the appropriate level for tests and full reporting of outcomes |
| <input checked="" type="checkbox"/> | <input type="checkbox"/> | Estimates of effect sizes (e.g. Cohen's d , Pearson's r), indicating how they were calculated |

Our web collection on [statistics for biologists](#) contains articles on many of the points above.

Software and code

Policy information about [availability of computer code](#)

Data collection

Data analysis https://doi.org/10.5281/zenodo.11043386"/>

For manuscripts utilizing custom algorithms or software that are central to the research but not yet described in published literature, software must be made available to editors and reviewers. We strongly encourage code deposition in a community repository (e.g. GitHub). See the Nature Portfolio [guidelines for submitting code & software](#) for further information.

Data

Policy information about [availability of data](#)

All manuscripts must include a [data availability statement](#). This statement should provide the following information, where applicable:

- Accession codes, unique identifiers, or web links for publicly available datasets
- A description of any restrictions on data availability
- For clinical datasets or third party data, please ensure that the statement adheres to our [policy](#)

https://doi.org/10.5281/zenodo.11043386"/>

Research involving human participants, their data, or biological material

Policy information about studies with [human participants or human data](#). See also policy information about [sex, gender \(identity/presentation\), and sexual orientation](#) and [race, ethnicity and racism](#).

Reporting on sex and gender	<input type="text" value="Not applicable to this work."/>
Reporting on race, ethnicity, or other socially relevant groupings	<input type="text" value="Not applicable to this work."/>
Population characteristics	<input type="text" value="Not applicable to this work."/>
Recruitment	<input type="text" value="Not applicable to this work."/>
Ethics oversight	<input type="text" value="Not applicable to this work."/>

Note that full information on the approval of the study protocol must also be provided in the manuscript.

Field-specific reporting

Please select the one below that is the best fit for your research. If you are not sure, read the appropriate sections before making your selection.

Life sciences Behavioural & social sciences Ecological, evolutionary & environmental sciences

For a reference copy of the document with all sections, see [nature.com/documents/nr-reporting-summary-flat.pdf](https://www.nature.com/documents/nr-reporting-summary-flat.pdf)

Ecological, evolutionary & environmental sciences study design

All studies must disclose on these points even when the disclosure is negative.

Study description	<input type="text" value="A study on how temperature affect the division rates and abundance of marine phytoplankton"/>
Research sample	<input type="text" value="Natural populations of marine cyanobacteria"/>
Sampling strategy	<input type="text" value="The sampling strategy involved collecting data from a variety of sources. Sample sizes were determined by the availability of data from different sources. The large sample size of the SeaFlow data and the compilation of division rate estimates were collected to ensure sufficient statistical power for the analyses."/>
Data collection	<input type="text" value="We used publicly available SeaFlow data, which includes cell size and abundance of small phytoplankton, as well as environmental variables: sea surface temperature, nutrient concentrations (nitrate, phosphate), and Photosynthetically Active Radiation (PAR) data We also used compiled data which include data from dilution experiments, cell cycle analysis and under controlled laboratory conditions extracted from published literature."/>
Timing and spatial scale	<input type="text" value="Data were collected from 2010 to 2023 across the tropical and subtropical Pacific and Atlantic Oceans (20°S to 30°N)"/>
Data exclusions	<input type="text" value="Data points with low-quality flags were excluded."/>
Reproducibility	<input type="text" value="The code and data are provided in this repository to ensure the reproducibility of the results. All attempts to repeat the analyses using the provided code and data were successful."/>
Randomization	<input type="text" value="Randomization is not relevant to study."/>
Blinding	<input type="text" value="The investigators were not blinded to allocation during experiments and outcome assessment."/>
Did the study involve field work?	<input checked="" type="checkbox"/> Yes <input type="checkbox"/> No

Field work, collection and transport

Field conditions	<input type="text" value="Data were collected in tropical and subtropical Pacific and Atlantic Oceans during 90 research cruises from 2010 to 2023, with temperatures ranging from 12 to 30°C."/>
Location	<input type="text" value="Data were collected in surface waters across 40°S to 40°N latitudes and 50 °E and 350°E longitudes"/>
Access & import/export	<input type="text" value="No physical biological samples were collected or imported/exported for this study. Cruise operations were conducted with full"/>

Access & import/export	cooperation of host institutions and followed standard oceanographic research protocols established by the research vessel operators and funding agencies.
Disturbance	All data collection activities were performed in accordance with the ethical guidelines of the University of Washington and collaborating institutions, ensuring minimal environmental impact through the use of existing ship infrastructure and non-invasive sampling methodologies.

Reporting for specific materials, systems and methods

We require information from authors about some types of materials, experimental systems and methods used in many studies. Here, indicate whether each material, system or method listed is relevant to your study. If you are not sure if a list item applies to your research, read the appropriate section before selecting a response.

Materials & experimental systems

n/a	Involvement in the study
<input checked="" type="checkbox"/>	<input type="checkbox"/> Antibodies
<input checked="" type="checkbox"/>	<input type="checkbox"/> Eukaryotic cell lines
<input checked="" type="checkbox"/>	<input type="checkbox"/> Palaeontology and archaeology
<input checked="" type="checkbox"/>	<input type="checkbox"/> Animals and other organisms
<input checked="" type="checkbox"/>	<input type="checkbox"/> Clinical data
<input checked="" type="checkbox"/>	<input type="checkbox"/> Dual use research of concern
<input checked="" type="checkbox"/>	<input type="checkbox"/> Plants

Methods

n/a	Involvement in the study
<input checked="" type="checkbox"/>	<input type="checkbox"/> ChIP-seq
<input checked="" type="checkbox"/>	<input type="checkbox"/> Flow cytometry
<input checked="" type="checkbox"/>	<input type="checkbox"/> MRI-based neuroimaging

Plants

Seed stocks	Natural populations of marine cyanobacteria
Novel plant genotypes	Not applicable to this work.
Authentication	Not applicable to this work.